Stem Cell Reports
Article

ISSCR

OPEN ACCESS

Rbbp4 Suppresses Premature Differentiation of Embryonic Stem Cells

Yikai Huang,[1] Ting Su,[1] Congcong Wang,[1] Lixia Dong,[1] Shuang Liu,[1] Yaru Zhu,[1] Kunying Hao,[1] Yin Xia,[2,*] Qing Jiang,[3,*] and Jinzhong Qin[1,*]

[1]State Key Laboratory of Pharmaceutical Biotechnology and MOE Key Laboratory of Model Animals for Disease Study, Model Animal Research Center, School of Medicine, Nanjing University, 12 Xuefu Road, Nanjing, Jiangsu 210061, China
[2]School of Biomedical Sciences, The Chinese University of Hong Kong, Hong Kong, China
[3]Department of Sports Medicine and Adult Reconstructive Surgery, Nanjing Drum Tower Hospital Affiliated to Medical School of Nanjing University, Nanjing, China
*Correspondence: xia.yin@cuhk.edu.hk (Y.X.), qingj@nju.edu.cn (Q.J.), qinjz@nju.edu.cn (J.Q.)
https://doi.org/10.1016/j.stemcr.2021.01.009

SUMMARY

Polycomb group (PcG) proteins exist in distinct multi-protein complexes and play a central role in silencing developmental genes, yet the underlying mechanisms remain elusive. Here, we show that deficiency of retinoblastoma binding protein 4 (RBBP4), a component of the Polycomb repressive complex 2 (PRC2), in embryonic stem cells (ESCs) leads to spontaneous differentiation into mesendodermal lineages. We further show that *Rbbp4* and core PRC2 share an important number of common genomic targets, encoding regulators involved in early germ layer specification. Moreover, we find that *Rbbp4* is absolutely essential for genomic targeting of PRC2 to a subset of developmental genes. Interestingly, we demonstrate that *Rbbp4* is necessary for sustaining the expression of *Oct4* and *Sox2* and that the forced co-expression of *Oct4* and *Sox2* fully rescues the pluripotency of *Rbbp4*-null ESCs. Therefore, our study indicates that *Rbbp4* links maintenance of the pluripotency regulatory network with repression of mesendoderm lineages.

INTRODUCTION

The polycomb group (PcG) proteins function as chromatin-based transcriptional repressors that are essential for the specification and maintenance of cell fates (Kuroda et al., 2020; Schuettengruber et al., 2017). They broadly assemble into two biochemically and functionally distinct chromatin-associated complexes, the polycomb repressive complexes 1 and 2 (PRC1 and PRC2). PRC1 mono-ubiquitylates histone H2A at position 119 (H2AK119ub1) using its E3 ubiquitin ligase subunits, RING1A/B. Multiple PRC1 sub-complexes have been identified, which are characterized by the incorporation of distinct PCGF homologs and versatile accessory partners and can be grouped into canonical and non-canonical PRC1 (cPRC1 and ncPRC1). The cPRC1 is composed of four core subunits: RING E3 ligase (RING1A/B), PCGF (Pcgf1–6), PHC (polyhomeotic homologs; PHC1/2/3), and CBX (polycomb; CBX2/4/6/7/8) (Di Croce and Helin, 2013; Simon and Kingston, 2009; Turner and Bracken, 2013). In ncPRC1 complexes, RYBP, or its paralog YAF2 replaces CBX and PHC subunits found in cPRC1s (Turner and Bracken, 2013).

PRC2 consists of four core proteins, SUZ12, EED, RBBP4/7, and either of the two histone H3K27 methyltransferases, EZH1 or EZH2, which mono-, di-, and tri-methylates histone H3 at lysine 27 (H3K27me1/2/3) (Margueron et al., 2008; Piunti and Shilatifard, 2016). In addition to the four core subunits, PRC2 interacts with several auxiliary components that fine-tune its enzymatic activity and/or modulate its recruitment to chromatin. The PRC2.1 contains one of the three PCL1–3 (Polycomb-like protein 1–3) paralogs, whereas PRC2.2 is characterized by the presence of AEBP2 together with JARID2 (Holoch and Margueron, 2017). Notably, it has long been thought that PRC2-mediated H3K27me3, recognized by a chromodomain-containing CBX protein subunit of cPRC1, is required for recruiting PRC1 at PcG repressed sites, providing a functional bridge between the two major PcG complexes. However, this view was challenged by the identification of ncPRC1 complexes, which lack H3K27me3-binding CBX subunits. Furthermore, recent studies have shown that the ncPRC1 complex, but not the cPRC1 complex, promotes H2AK119ub-dependent recruitment of PRC2, suggesting a critical role for ncPRC1 in PcG-mediated gene control (Blackledge et al., 2014).

Mice deficient for *Suz12*, *Ezh2*, or *Eed* exhibited embryonic lethality due to gastrulation defects (Faust et al., 1998; O'Carroll et al., 2001; Pasini et al., 2004), underscoring the importance of these core components of PRC2 in early embryogenesis. In line with this, embryonic stem cells (ESCs) lacking *Ezh2*, *Eed*, and *Suz12*, were deficient in somatic cell reprogramming by cell fusion (Pereira et al., 2010a). Interestingly, ESCs deficient for *Suz12*, *Eed*, or *Ezh2* appear to be normal with little effect on morphology and self-renewal, indicating that PRC2 may be dispensable for overall maintenance of pluripotency (Chamberlain et al., 2008; Montgomery et al., 2005; Pasini et al., 2007). It is worth highlighting here that functional redundancy among members of the PRC2 complex could account for the mild to no phenotype of mutants lacking individual PRC2 subunits in ESCs.

Retinoblastoma binding protein 4 (RBBP4) and RBBP7 are a pair of WD40 motif containing proteins sharing a

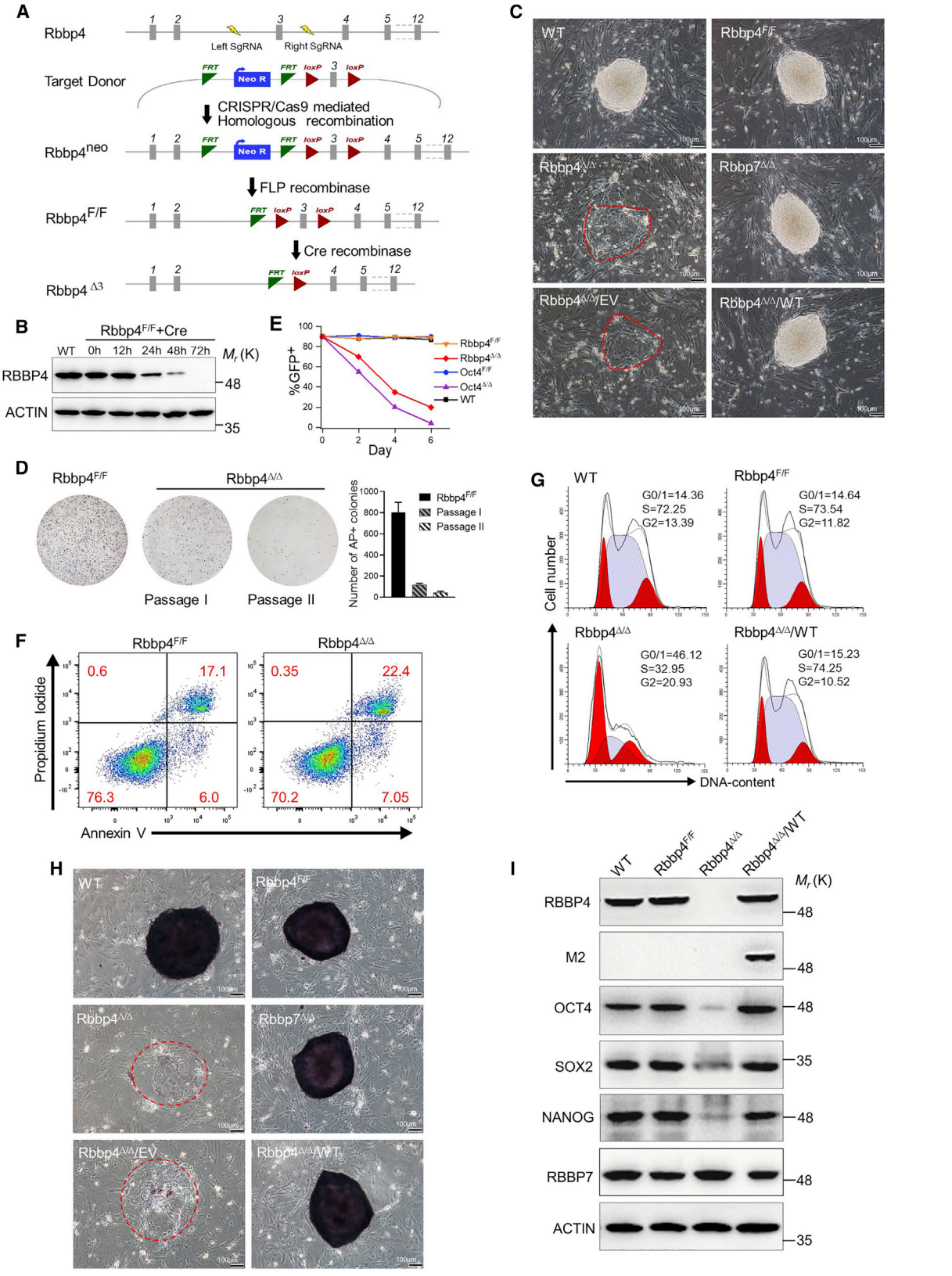

(legend on next page)

sequence identity of 92%, which often exist together in multiple chromatin modifying complexes, such as the PRC2 (Conway et al., 2018), the NuRD complex (Feng and Zhang, 2003), and Sin3/HDAC complex (Kuzmichev et al., 2002). WD40 domain proteins are involved in a variety of fundamental biological processes, in which WD40 domains, containing 40–60 residues with a defining tryptophan-aspartate (WD) dipeptide, serve as scaffolds for complex assembly or provide platforms to recruit diverse molecules that form functional complexes. A recent study indicated that *Rbbp4* is essential for early embryonic development in mice (Miao et al., 2020). However, the exact cause of early embryonic lethality of *Rbbp4* knockouts and its potential roles in maintenance of stem cells or pluripotency have not been studied.

In this report, we demonstrate that ablating *Rbbp4* gene expression in ESCs results in a loss of the undifferentiated state and the initiation of differentiation along mesendodermal lineage. Mechanistically, we demonstrate that *Rbbp4* plays an important role in guiding the PRC2 to the loci of developmental genes where they establish and maintain the repressive states of lineage-specific genes in ESCs. Our study therefore identifies RBBP4 as an essential chromatin factor for the maintenance of ESC pluripotency and shows that it functions within the PRC2 complex to repress mesendoderm specification.

RESULTS

Rbbp4 is essential in the maintenance of self-renewal and pluripotency in ESCs

To circumvent the potential lethality that results from complete loss of *Rbbp4* and to gain insight into the role of this gene in ESCs, we generated *Rbbp4* conditional knockout mouse ESCs (Figures 1A and S1A–S1C), in which the third coding exon of both *Rbbp4* alleles was flanked by parallel *loxP* sites, based on Cre-*loxP* system. In this *Rbbp4* conditional floxed ESC line ($Rbbp4^{F/F}$), *Rbbp4* was completely removed 72 h after transfection with a plasmid encoding Cre, as evident in western blot (Figures 1B and S1D). Therefore, the cells were used for assay after 72 h of transfection throughout this study unless otherwise stated in the figure legends. Notably, $Rbbp4^{F/F}$ showed normal RBBP4 protein levels and formed robust colonies that were morphologically indistinguishable from wild-type ESCs. However, as shown in Figure 1C, in contrast to the $Rbbp4^{F/F}$, ablation of *Rbbp4* resulted in flat and spreading colonies without smooth edges. Importantly, ablation of *Rbbp4* dramatically decreased secondary ES colony formation (Figure 1D). Consistently, in ESC competition assays, complete abolishment of *Rbbp4* resulted in loss of self-renewal similar to deletion of *Oct4* (Figure 1E). $Rbbp4^{\Delta/\Delta}$ ESCs displayed the same apoptotic rates as the $Rbbp4^{F/F}$, as shown by annexin V staining (Figure 1F). Cell-cycle analysis revealed cells lacking *Rbbp4* have a markedly extended G1 phase and a shortened S phase, suggesting that the impaired growth of $Rbbp4^{\Delta/\Delta}$ ESCs was due to an altered cell-cycle profile (Figure 1G). After alkaline phosphatase (AP) staining, $Rbbp4^{F/F}$ as well as wild-type ESC colonies stained bright and uniform, while the $Rbbp4^{\Delta/\Delta}$ colonies appeared dim, weak, and mosaic, suggesting loss of ESC self-renewal capability (Figure 1H). Consistent with the AP staining results, the expression of pluripotency genes *Oct4*, *Sox2*, and *Nanog* dramatically declined upon loss of *Rbbp4* gene expression (Figure 1I). Importantly, lentivirus-mediated delivery of FLAG-tagged full-length *Rbbp4* fully rescued the defective phenotypes associated with *Rbbp4* deficiency. Remarkably, the complete loss of *Rbbp7* (Figures S2A–S2E), which shares 92% of sequence identity with *Rbbp4*, caused no detectable defects in ESCs (Figures 1C and 1H). Together, these data indicate that *Rbbp4* plays an important role in governing the pluripotent state in ESCs.

Figure 1. *Rbbp4* is essential in the maintenance of self-renewal and pluripotency in ESCs

(A) Schematic representation of the production for conditional inactivation of *Rbbp4* in ESCs.

(B) Western blot showing RBBP4 levels in $Rbbp4^{F/F}$-transfected Cre recombinase for different time points.

(C) Morphology of ESC colonies of indicated genotypes. Bright-field images of ESC colonies after 7 days of culture (grown from a single ESC). All ESC colony images were photographed at day 7 after seeding single-cell suspensions on feeder layers. Scale bar, 100 μm. The outlines of obviously defective colonies were circled in red. $Rbbp4^{\Delta/\Delta}$ ESCs expressing empty FLAG vector ($Rbbp4^{\Delta/\Delta}$/*EV*) and vectors encoding wild-type RBBP4-FLAG ($Rbbp4^{\Delta/\Delta}$/*WT*) are also shown.

(D) Secondary ES colony-replating assay. Bar graph shows the number of cells with AP-positive staining in the absence of RBBP4. Error bars represent means and STD from three 6 cm dishes.

(E) ESC growth competition assay. *Oct4* knockout ESCs serve as a negative control.

(F) Representative fluorescence-activated cell sorting plots of annexin V and propidium iodide (PI) levels in $Rbbp4^{F/F}$ and $Rbbp4^{\Delta/\Delta}$ ESCs. Percentages of cells with different apoptosis marker levels are shown.

(G) Cell-cycle analysis of indicated ESCs. Percentages of cells in different phases are indicated. Representative histograms presented here show distribution of cells in sequential phases (G0/G1, red; S, light blue; and G2/M, red) of cell cycle.

(H) Alkaline phosphatase activity staining on each indicated ESC colony. Scale bar, 100 μm.

(I) Western blot analysis of OCT4, SOX2, NANOG, RBBP4, and RBBP7 protein expression in indicated ESCs; ACTIN served as a loading control. See also Figures S1 and S2.

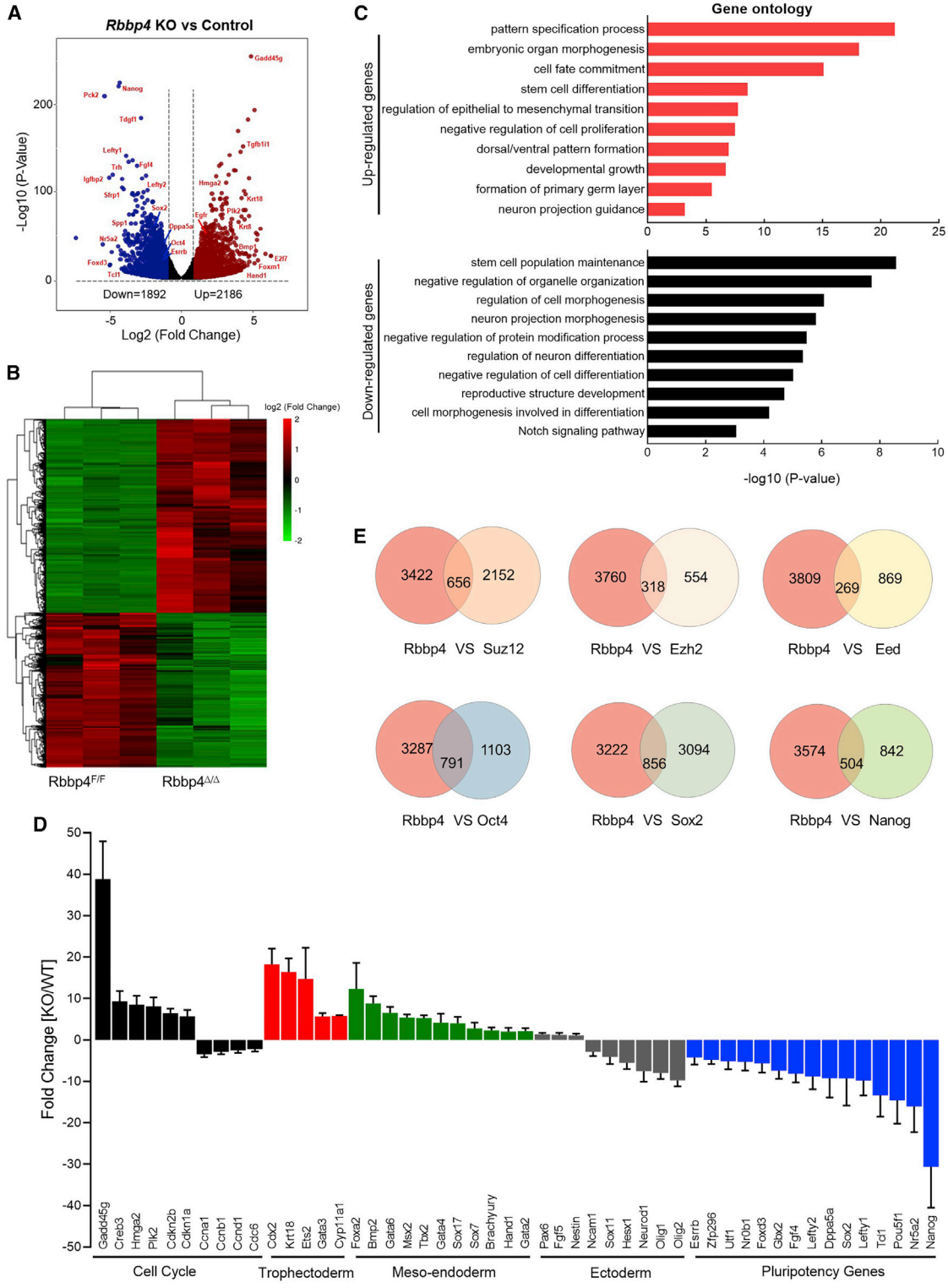

Figure 2. Loss of *Rbbp4* results in aberrant expression of ESC core pluripotency factors and differentiation-associated genes

(A) Volcano plot showing the distribution of the differentially expressed (DE) genes with 2-fold changes upon *Rbbp4* deletion. $p < 0.05$. Up- and downregulated genes are colored red and blue, respectively.

(legend continued on next page)

Loss of *Rbbp4* results in aberrant expression of ESC core pluripotency factors and differentiation-associated genes

To explore the molecular basis of phenotypic alterations observed in *Rbbp4*-null ESCs and to rule out the possibility that loss of the undifferentiated state and self-renewal observed in $Rbbp4^{\Delta/\Delta}$ ESCs was due to a general impairment in cell proliferation, we performed gene expression analysis for $Rbbp4^{F/F}$ and $Rbbp4^{\Delta/\Delta}$ ESCs by RNA sequencing (RNA-seq) analysis. There were 4,078 genes that were differentially expressed by more than 2-fold upon *Rbbp4* ablation (Figures 2A and 2B). About an equal number of genes were upregulated (2,186) or downregulated (1,892) in $Rbbp4^{\Delta/\Delta}$ ESCs. Gene ontology (GO) analysis showed that among genes downregulated in $Rbbp4^{\Delta/\Delta}$ ESCs were genes related to stem cell population maintenance, regulation of cell morphogenesis, and negative regulation of cell differentiation. Processes related to cell fate commitment, stem cell differentiation, pattern specification process, and tissue morphogenesis, were over-represented among the genes upregulated in the $Rbbp4^{\Delta/\Delta}$ ESCs (Figure 2C). By performing qRT-PCR analysis, we confirmed the differential expression of selected genes observed by RNA-seq analysis and showed that, while the expression of these genes was significantly reduced or increased in $Rbbp4^{\Delta/\Delta}$ ESCs (Figure 2D), their expression was largely unaffected in $Rbbp7^{\Delta/\Delta}$ ESCs (data not shown). Importantly, among $Rbbp4^{\Delta/\Delta}$ downregulated genes, our analysis revealed the pluripotency signature genes and transcription factors, including *Oct4* (*Pou5f1*), *Sox2*, *Nanog*, *Nr5a2*, *Dppa5a*, and *Esrrb* (Figure 2D), which were shown to have critical roles in maintaining pluripotency in ESCs. In addition, qRT-PCR analysis of several lineage-specific markers demonstrated that loss of *Rbbp4* led to the upregulation of mesendoderm markers (*Foxa2*, *Gata6*, *Gata4*, *Sox17*, *Brachyury*, *Msx2*, and *Tbx2*) and trophectoderm markers (*Cdx2*, *Ets2*, *Gata3*, and *Krt18*), whereas ectoderm markers (*Pax6*, *Sox11*, *Neurod1*, *Olig1*, and *Olig2*) were instead either unchanged or slightly decreased (Figure 2D). Consistent with our cell-cycle analysis (Figure 1G), we found a substantial number of genes involved in proliferation to be differentially expressed in $Rbbp4^{\Delta/\Delta}$ cells. These include $p21^{WAF1/CIP1}$, a potent inducer of G1 arrest, and members of the cyclin family, key regulators in cell-cycle machinery (Figure 2D). Interestingly, deficiency of Rbbp4 in ESCs was associated with substantially reduced levels of the phosphorylated and hyperphosphorylated (ppRb) forms of the Rb protein at several residues (Figure S3A). As expected, a large number of the genes de-regulated in $Rbbp4^{\Delta/\Delta}$ cells was also observed in ESCs deficient for *Suz12*, *Ezh2*, and *Eed* (Figure 2E), consistent with the idea that they exist in the same complex. Moreover, transcriptional changes in $Rbbp4^{\Delta/\Delta}$ cells significantly overlapped with those seen in *Oct4*-, *Sox2*-, or *Nanog*-deficient ESCs, and those overlapping genes were enriched for pluripotency and cell differentiation. Altogether, the evidences collected so far clearly suggest that *Rbbp4* has key roles in controlling the pluripotent state of ESCs.

RBBP4 shares target genes with PRC2

Given the rapid changes in gene expression patterns observed in $Rbbp4^{\Delta/\Delta}$ ESCs, we hypothesized that *Rbbp4* may directly regulate both pluripotency and lineage-specific genes. We performed chromatin immunoprecipitation followed by high-throughput sequencing (ChIP-seq) analysis of RBBP4 binding. We found that the RBBP4 protein bound to 2,804 sites. A total of 16.1% of these sites were around gene promoters (defined as up to 2 kb upstream from the transcription start sites of the gene), 44% were within gene coding sequences, and 39.9% were intergenic-enhancer binding sites (Figure 3A). Thus, our analyses suggest that, on the genome, RBBP4 is mostly present at distal intergenic and intronic regions. Interestingly, GO analysis showed significant enrichment in genes involved in neuron development, pattern specification process, and regulation of cell differentiation (Figure 3B), strikingly resembling classical GO of PRC2 targets (Pereira et al., 2010b). Comparison of the de-regulated genes in $Rbbp4^{\Delta/\Delta}$ cells with the occupancy of RBBP4 in ESCs revealed that, among 2,186 genes that were upregulated in $Rbbp4^{\Delta/\Delta}$, 218 genes were bound by RBBP4, whereas 132 of 1,892 downregulated genes were RBBP4 bound (Figure 3C). GO

(B) Heatmap illustrating the RNA expression in $Rbbp4^{F/F}$ and $Rbbp4^{\Delta/\Delta}$ ESCs of RNA-seq analysis for 2-fold expression differentially expressed genes. False discovery rate < 0.05. Up- and downregulated genes are reported as red and green, respectively.

(C) Gene ontology (GO) enrichment analyses for biological processes associated with genes differentially expressed upon *Rbbp4* deletion in ESCs. Analysis was carried out using Metascape (Zhou et al., 2019).

(D) Validation of RNA-seq data by qRT-PCR analysis. Relative mRNA levels of indicated cell-cycle-related genes, lineage-specific genes, and pluripotency-related genes in $Rbbp4^{F/F}$ after 3 days of Cre transfection were measured and data were normalized to β-actin relative to $Rbbp4^{F/F}$. Data are pooled from three independent experiments and the error bars represent standard deviation of triplicate qPCR data.

(E) Venn diagrams (top) showing the overlap of the target genes between *Rbbp4* and the core subunits of the PRC2 complex, respectively (Das et al., 2015; Pasini et al., 2007). Venn diagrams (bottom) showing the numbers of the regulated genes between *Rbbp4* and pluripotency markers (*Oct4*, *Sox2*, and *Nanog*) (Ding et al., 2015; Loh et al., 2006).

See also Figure S3.

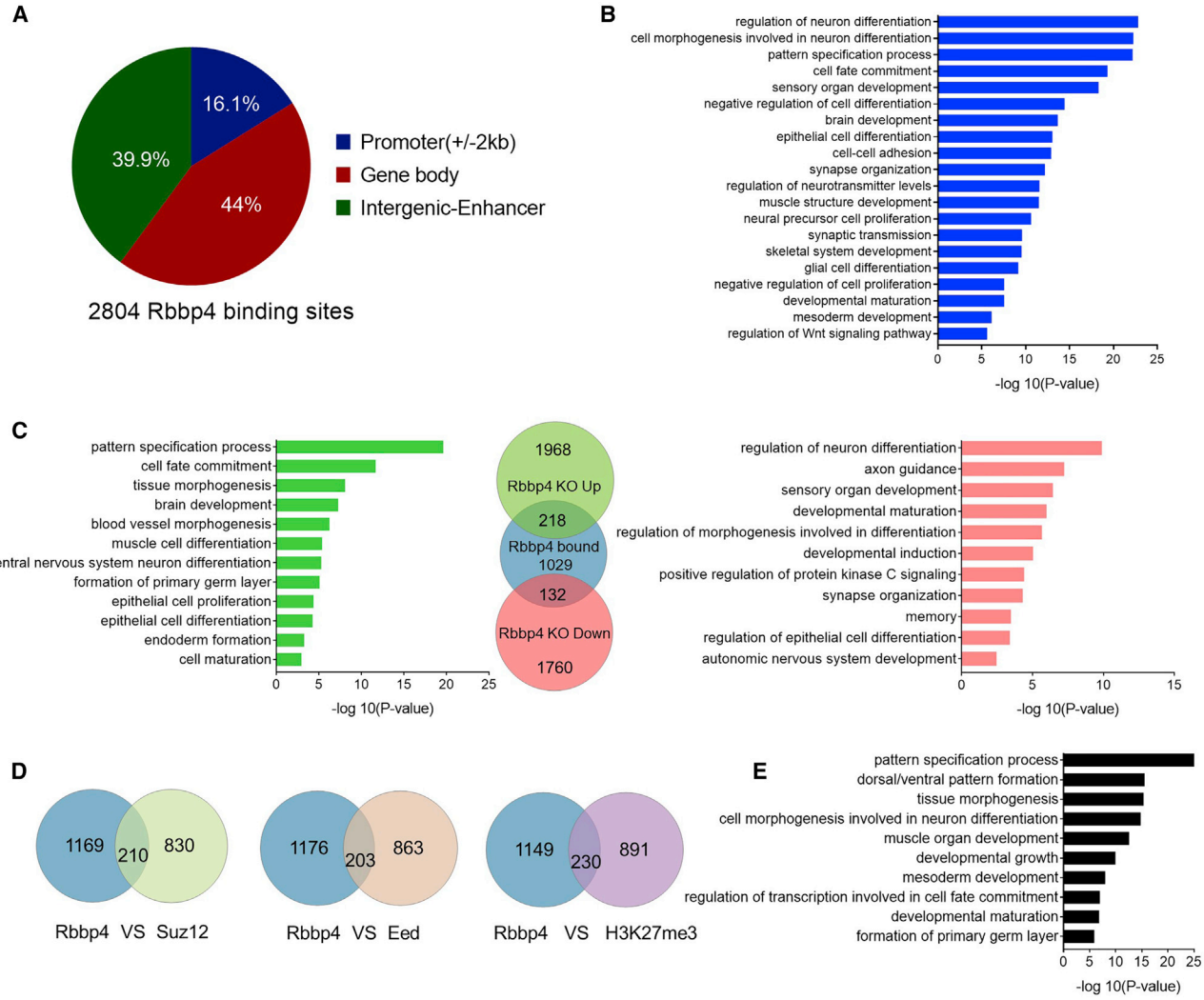

(legend on next page)

analysis of these overlapping genes again demonstrated a strong enrichment of terms involved in neuron differentiation, cell fate commitment, and pattern specification process. Since RBBP4 is physically associated with PRC2, as expected, we found that 210, 203, or 230 of *Rbbp4* targets are also bound by SUZ12, EED, and H3K27me3, respectively (Figure 3D). Many of these genes were known critical regulators of pattern specification process, primary germ layer formation, cell fate commitment, and neuron differentiation (Figure 3E). Importantly, a detailed examination of RBBP4 ChIP-seq revealed that RBBP4 bound to the promoters of a group of genes associated with pluripotency or mesendodermal differentiation (Figure 3F).

To identify the regions within the RBBP4 protein that are required for its chromatin targeting, we generated a set of FLAG-tagged *Rbbp4* deletion mutants and introduced them into $Rbbp4^{F/F}$ ESCs (Figure S4A). Notably, all mutants were expressed at similar levels as evaluated by western blotting (Figure S4B). To test whether these mutants could retain recruitment to targets and to examine the ability of these mutants to maintain the expression of *Rbbp4* target genes in the absence of endogenous *Rbbp4*, the cells were transduced with Cre recombinase and assayed 14 days later. ChIP-qPCR analyses demonstrated that the N-terminally deleted protein and the mutants with deletion of WD40 domains (individual or tandem), did not bind to targets (Figures S4C and S4D). Consistent with their failure to bind chromatin in ESCs, these mutants also lost the ability to restore target gene expression (Figure S4E). In contrast, the C terminus of RBBP4 was dispensable for binding and thus maintain these gene expressions as effectively as the wild type. To gain insight into the ability of these mutants to rescue self-renewal defect observed in $Rbbp4^{\Delta/\Delta}$ ESCs, we analyzed their ability to produce colonies after seeding on mouse embryonic fibroblasts (MEFs). As shown in Figures S4F–S4H, C-terminal deletion mutants fully rescued wild-type levels of growth in ESCs. However, RBBP4 lacking the WD40 domains or N-terminal virtually abolished its ability to restore the colony growth defect. Taken together, these results indicate that both N-terminal and WD40 domains are essential for the chromatin targeting of RBBP4 and show that these regions confer upon RBBP4 the capacity to control ESC properties.

Rbbp4 governs pluripotency via maintaining the expression of *Oct4* and *Sox2*

To evaluate transcriptional mediators responsible for loss of pluripotency and lineage specification upon *Rbbp4* deficiency, we examined the temporal mRNA expression of pluripotency-related genes as well as three germ layer marker genes in $Rbbp4^{F/F}$ ESCs after transfection with Cre. As shown in Figure 4A, real-time qRT-PCR analysis revealed that *Oct4*, *Sox2*, and *Nanog* mRNA levels significantly decreased within 3 days after *Rbbp4* ablation and declined steadily thereafter to baseline levels on day 7. In contrast, mesendoderm markers (*Gata4*, *Gata6*, *Sox17*, *Hand1*, *Msx2*, and *Brachyury*) and trophectoderm markers (*Cdx2* and *Gata3*) were upregulated at the same time point that the mRNA of core pluripotency factors decreased. The precocious differentiation of $Rbbp4^{\Delta/\Delta}$ ESCs was also monitored by immunofluorescence microscopy to detect the expression profile of germ layer markers alongside pluripotency factors (Figure 4B). In $Rbbp4^{F/F}$ ESCs, OCT4, SOX2, and NANOG expression was high, whereas positivity for FOXA2, GATA6, and CDX2 was rarely observed, indicating the undifferentiated state of the cells. After transient transfection of a Cre recombinase expression plasmid, FOXA2, GATA6, and CDX2 expression gradually increased in a time-dependent manner, which was accompanied by the decreased expression of a panel of pluripotency genes.

We found RBBP4 binding enrichment at genes encoding critical components of the pluripotency network, such as *Klf4*, *Sox2*, and *Oct4*, whose expression is downregulated upon *Rbbp4* ablation (Figures 3F, 4A, and S4C). These observations support the notion that *Rbbp4* silences differentiation programs in ESCs through regulation of these genes. Therefore, it would be extremely interesting to know if the defects observed in $Rbbp4^{\Delta/\Delta}$ ESCs depend on lack of *Oct4*, *Nanog*, or *Sox2* repression. To this end, we attempted to rescue $Rbbp4^{\Delta/\Delta}$ ESCs by introducing the transgenes of *Oct4*, *Nanog*, or *Sox2*. The *Rbbp4*-null rescue system utilized

Figure 3. RBBP4 shares target genes with PRC2

(A) Pie chart showing the distribution of RBBP4 binding sites in mouse ESCs.

(B) GO enrichment analyses for genes that RBBP4 binds to. The biological processes of the top 20 are shown.

(C) Venn diagram showing the overlap between genes differentially expressed after Rbbp4 deletion and those occupied by RBBP4. GO analysis for biological processes associated with the overlapping genes.

(D) Venn diagram showing the overlap between genes that RBBP4 binds to and those occupied by SUZ12, EED, or H3K27me3.

(E) GO analysis of overlapping genes between RBBP4 binds and PRC2 targets.

(F) Genome browser tracks to show RBBP4 occupancy near lineage-specific markers for trophectoderm (Cdx2), mesoderm (Brachyury, Tbx2), and endoderm (Sox17, Gata4), Oct4 and Sox2 (up). ChIP-qPCR data showing binding of RBBP4-FLAG to representative RBBP4 target promoters (bottom).

Data are plotted as mean ± SD. (n = 3). *$p < 0.05$, **$p < 0.01$. See also Figure S4.

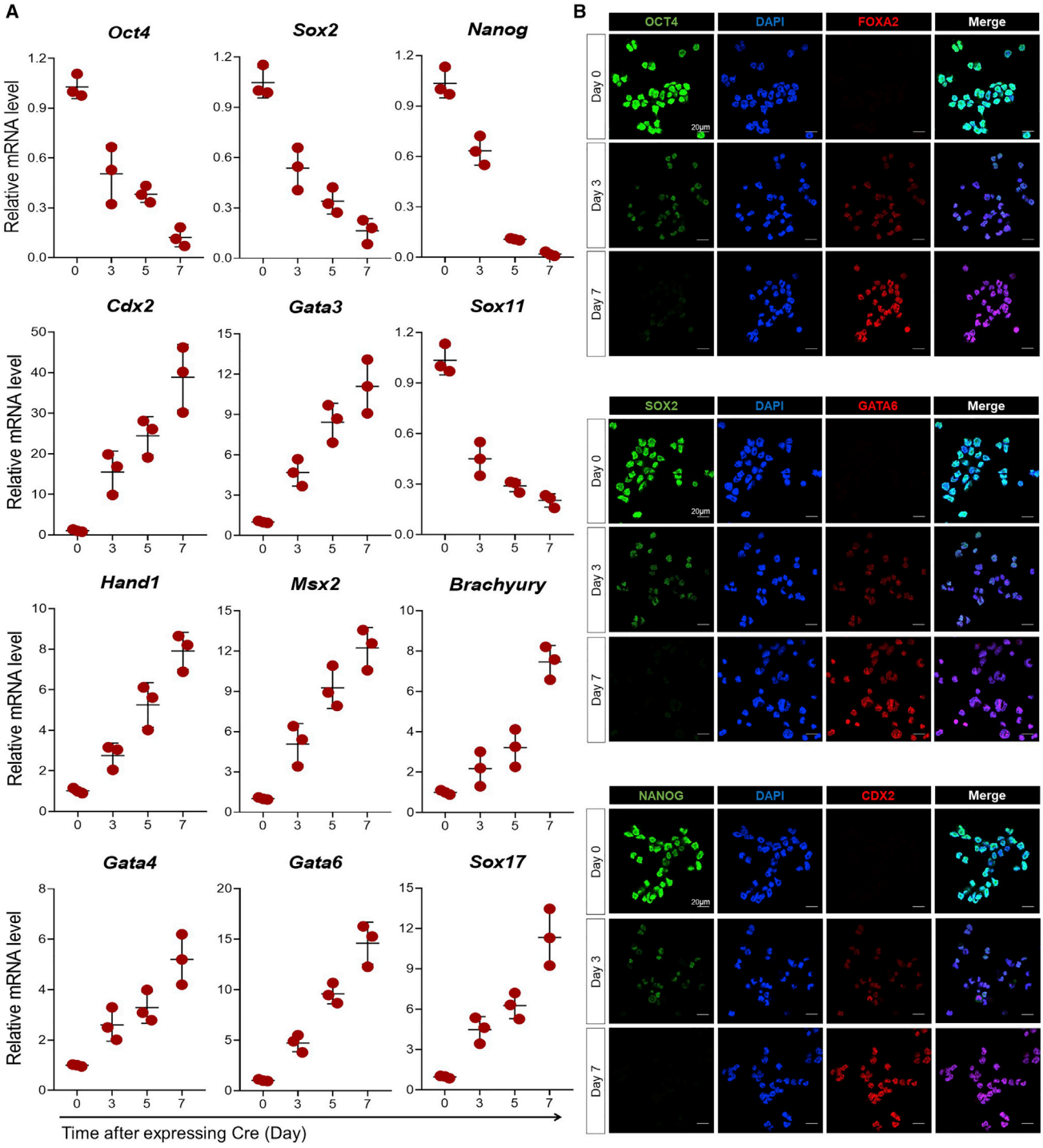

Figure 4. *Rbbp4* knockout significantly reduces the expression of pluripotency-associated genes and promotes mesendodermal gene expression in ESCs

(A) Time-course analyses of pluripotency-associated genes and the lineage-specific markers for trophectoderm, mesoderm, and endoderm expression levels in *Rbbp4*$^{F/F}$ ESCs after transient expression of Cre recombinase. Expression is normalized by β-actin.

(legend continued on next page)

Rbbp4$^{F/F}$ ESCs, in which the floxed *Rbbp4* alleles were excised by Cre recombinase (Figure 5A). Introducing *Nanog* (*Rbbp4*$^{\Delta/\Delta}$/*Nanog*) did not significantly restore the self-renewal defect observed in *Rbbp4*$^{\Delta/\Delta}$ ESCs, but introducing either the *Oct4* (*Rbbp4*$^{\Delta/\Delta}$/*Oct4*) or *Sox2* (*Rbbp4*$^{\Delta/\Delta}$/*Sox2*) transgenes successfully partially rescued the propagation of *Rbbp4*$^{\Delta/\Delta}$ ESCs. Most importantly, forced (ectopic) expression of both *Oct4* and *Sox2* together (*Rbbp4*$^{\Delta/\Delta}$/*Oct4*/*Sox2*) completely rescued the proliferation defect of *Rbbp4*-deficient ESCs (Figures 5B–5E). The *Rbbp4*$^{\Delta/\Delta}$/*Oct4*, *Rbbp4*$^{\Delta/\Delta}$/*Sox2*, or *Rbbp4*$^{\Delta/\Delta}$/*Oct4*/*Sox2* cells were able to form viable colonies on feeder cells and expand continuously for at least 50 passages without any significant change in colony morphology. It is worth noting that, although these three rescued lines exhibited similar expression levels of *Oct4* and *Sox2* (Figure 5F), the expression levels of other pluripotency-associated genes, such as *Fgf4*, *Dppa5a*, *Utf1*, *Lefty1*, *Nr5a2*, and *Tcl1*, in *Rbbp4*$^{\Delta/\Delta}$/*Oct4* or *Rbbp4*$^{\Delta/\Delta}$/*Sox2* were relatively higher than those in *Rbbp4*$^{\Delta/\Delta}$/*Oct4*/*Sox2* (Figure 5G).

We next examined the potential of these rescued cells to undergo *in vitro* differentiation. *Rbbp4*$^{\Delta/\Delta}$/*Oct4*, *Rbbp4*$^{\Delta/\Delta}$/*Sox2*, or *Rbbp4*$^{\Delta/\Delta}$/*Oct4*/*Sox2* and control ESCs were tested for their capacity to form embryoid bodies (EBs) (Figure 6A). *Rbbp4*$^{\Delta/\Delta}$ ESCs failed to form EBs. However, as shown in Figures 6B and 6C, *Rbbp4*$^{\Delta/\Delta}$/*Oct4*/*Sox2* ESCs produce EBs comparable with those of the wild type in size. *Rbbp4*$^{\Delta/\Delta}$/*Oct4* or *Rbbp4*$^{\Delta/\Delta}$/*Sox2* had the capacity to form EBs, but they were greatly reduced in size than those of the wild type during the differentiation process. In addition, qRT-PCR analysis revealed that *Rbbp4*$^{\Delta/\Delta}$/*Oct4* or *Rbbp4*$^{\Delta/\Delta}$/*Sox2* EBs expressed reduced mRNA levels of marker genes for the three germ layers (endoderm, mesoderm, and ectoderm), whereas the expression levels of these germ layer markers in *Rbbp4*$^{\Delta/\Delta}$/*Oct4*/*Sox2* EBs were similar to that of wild type (Figure 6D). In contrast to the expression of these germ layer-specific genes, pluripotency-related genes, namely *Oct4*, *Nanog*, and *Sox2*, were sharply depleted during the course of wild-type and *Rbbp4*$^{\Delta/\Delta}$/*Oct4*/*Sox2* EB differentiation, while *Rbbp4*$^{\Delta/\Delta}$/*Oct4* or *Rbbp4*$^{\Delta/\Delta}$/*Sox2* EB exhibited similar trends, but of a lesser magnitude (Figure 6E). Consistent with these results, teratomas derived from wild-type and *Rbbp4*$^{\Delta/\Delta}$/*Oct4*/*Sox2* ESCs contained multiple tissue types from all three germ layers, whereas *Rbbp4*$^{\Delta/\Delta}$/*Oct4* or *Rbbp4*$^{\Delta/\Delta}$/*Sox2* teratomas lacked ectodermal, endodermal, and mesodermal structures (Figures 6F and 6G). The differentiation defects observed in *Rbbp4*$^{\Delta/\Delta}$/*Oct4* or *Rbbp4*$^{\Delta/\Delta}$/*Sox2* might be due to higher expression levels of a subset of pluripotency-associated genes.

RBBP4 guides PRC2 recruitment and H3K27 trimethylation at genomic loci

RBBP4 has been found to exist in a complex with PRC2 (Conway et al., 2018). ESCs lacking a single component of the PRC2 complex, such as *Eed*, *Ezh2*, or *Suz12*, show marginal disruption of self-renewal (Chamberlain et al., 2008). However, the functional redundancy among the members of the PRC2 complex has not yet been addressed. To characterize the ability of each PRC2 member to support the self-renewal of ESCs, we generated individual or combined PRC2-deficient ESC lines by using CRISPR-Cas9 technology (Figures S5A–S5J and S6A–S6I) and analyzed their ability to form colonies after seeding on mitotically inactivated MEFs. The ESCs deficient for each of the PRC2 subunits were viable and formed dome-shaped undifferentiated AP-positive colonies, which were morphologically indistinguishable from those formed by wild-type cells (Figure 7A). In addition, the lack of deficits in ESC proliferation in *Ezh1*, *Jarid2*, and *Phf1*, or their closest family members *Ezh2*, *Aebp2*, and *Mtf2*/*Phf19*, respectively, single knockout is not likely caused by each other's compensation because double or triple knockout ESCs (*Ezh1*$^{\Delta/\Delta}$; *Ezh2*$^{\Delta/\Delta}$, *Jarid2*$^{\Delta/\Delta}$; *Aebp2*$^{\Delta/\Delta}$, or *Phf1*$^{\Delta/\Delta}$; *Mtf2*$^{\Delta/\Delta}$; *Phf19*$^{\Delta/\Delta}$) did not display significantly worse defects than single knockout ESCs. However, quadruple PRC2 knockout ESCs (*Ezh1*$^{\Delta/\Delta}$; *Ezh2*$^{\Delta/\Delta}$; *Eed*$^{\Delta/\Delta}$; *Suz12*$^{\Delta/\Delta}$) exhibited reduction of both colony number and size with an increased proportion of partially and fully differentiated populations and reduced AP activity, suggestive of a degree of functional redundancy among core members of the PRC2 family (Figures 7A and S5K-S5M). Interestingly, the mesendoderm (*Brachyury*, *Msx2*, *Gata4*, *Gata6*, and *Sox17*) and trophectoderm genes (*Cdx2*) in *Ezh1*$^{\Delta/\Delta}$; *Ezh2*$^{\Delta/\Delta}$; *Eed*$^{\Delta/\Delta}$; *Suz12*$^{\Delta/\Delta}$ ESCs reached similar levels as those in *Rbbp4*$^{\Delta/\Delta}$ ESCs, suggesting that the induction of this lineage-specific gene expression is the result of loss of function of the PRC2 complex in which RBBP4 is a component. These lineage-specific genes also showed significant elevations in their expression levels in *Suz12*$^{\Delta/\Delta}$, *Eed*$^{\Delta/\Delta}$, or *Ezh1*$^{\Delta/\Delta}$; *Ezh2*$^{\Delta/\Delta}$ ESCs, although the magnitude of the elevation was not as prominent as that observed in *Rbbp4*$^{\Delta/\Delta}$ ESCs (Figure 7B). However, no such induction was evident in *Jarid2*$^{\Delta/\Delta}$; *Aebp2*$^{\Delta/\Delta}$ or *Phf1*$^{\Delta/\Delta}$; *Mtf2*$^{\Delta/\Delta}$; *Phf19*$^{\Delta/\Delta}$ ESCs. The distinct phenotypes observed

(B) Immunofluorescence showing co-staining of the pluripotency markers (OCT4, SOX2, and NANOG) and the lineage-specific markers (FOXA2, GATA6, and CDX2) at the indicated time points after expressing Cre recombinase in *Rbbp4*$^{F/F}$ ESCs, respectively. DAPI (blue), pluripotency marker genes (green), the lineage-specific markers (red), and the merge picture are shown. Magnification, 63×.
Data are represented as mean ± SD of three independent experiments.

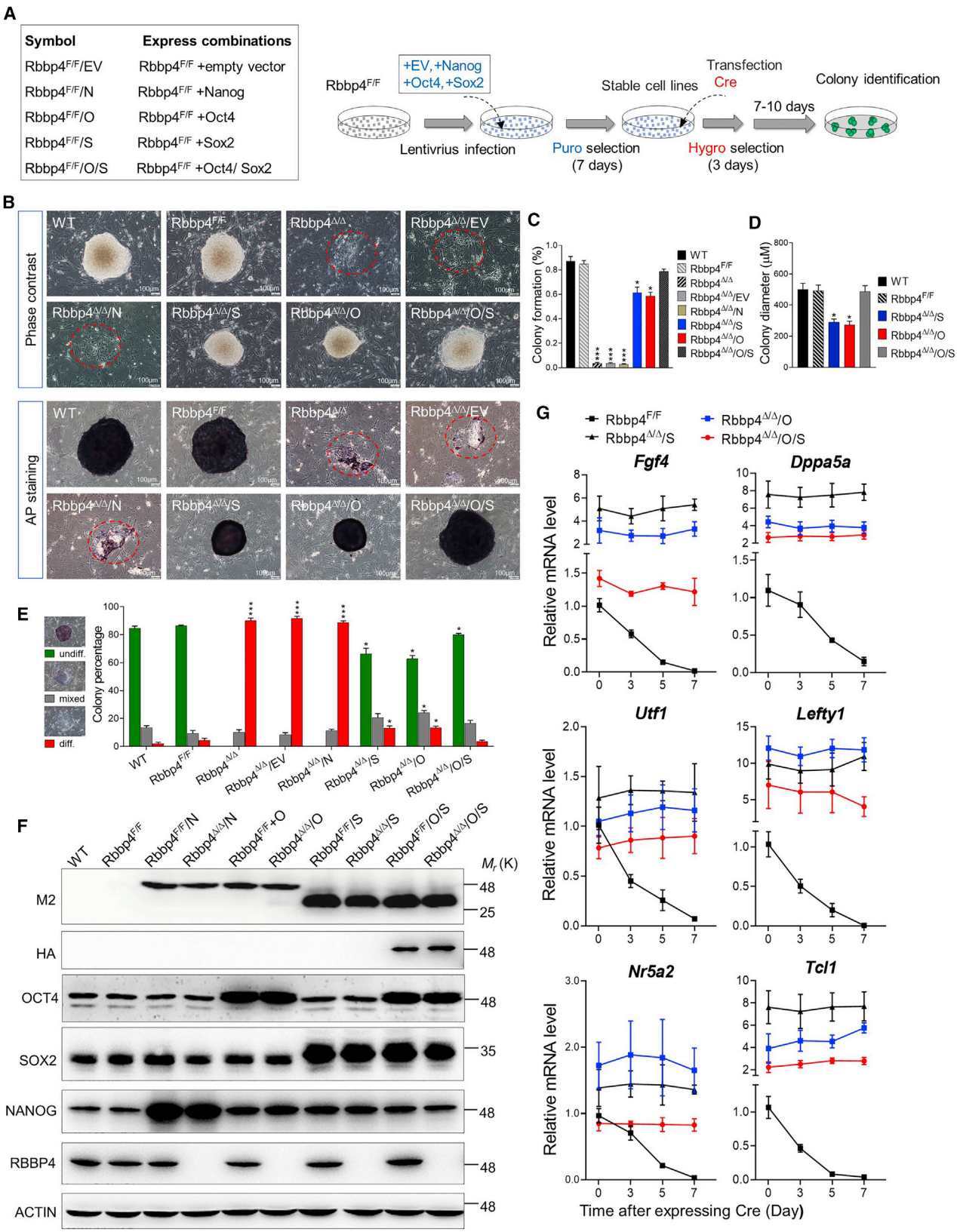

(legend on next page)

in *Ezh1*$^{\Delta/\Delta}$; *Ezh2*$^{\Delta/\Delta}$; *Eed*$^{\Delta/\Delta}$; *Suz12*$^{\Delta/\Delta}$, *Jarid2*$^{\Delta/\Delta}$; *Aebp2*$^{\Delta/\Delta}$, or *Phf1*$^{\Delta/\Delta}$; *Mtf2*$^{\Delta/\Delta}$; *Phf19*$^{\Delta/\Delta}$ ESCs strongly suggest that additional recruitment mechanisms contribute to recruiting the PRC2 complex to its genomic targets.

To confirm the interaction between RBBP4 and PRC2 core members, we performed endogenous coimmunoprecipitation experiments in ESCs and demonstrated that RBBP4 coprecipitated RBBP7, EZH1, EZH2, EED, and SUZ12. Importantly, immunoprecipitation analysis for SUZ12 in *Rbbp4*$^{\Delta/\Delta}$ ESCs revealed that *Rbbp4* ablation did not affect the association of core PRC2 components (Figure 7C). Furthermore, as shown in Figure 7D, *Rbbp4* deletion did not appear to adversely affect the protein levels of the components of PRC2. We next examined a possible cooperation between RBBP4 and PRC2 at the chromatin level. Thus, we analyzed PRC2 at its target genes in *Rbbp4*$^{\Delta/\Delta}$ ESCs by utilizing ChIP-qPCR assays. These experiments showed an impairment of genomic EZH2, SUZ12, and EED binding at target loci that we examined in the absence of RBBP4 but not RBBP7, accompanied by a dramatic decrease in H3K27me3 (Figure 7E). The global H3K27me3 levels were similar in wild type (Figure 7F), *Rbbp4*$^{F/F}$, and *Rbbp4*$^{\Delta/\Delta}$ ESCs, showing that the observed reduction of H3K27me3 at the PRC2 target promoters is due to changes in local EZH1/2 deposition. Collectively, these results demonstrate that RBBP4 is absolutely crucial for genomic loading of the entire PRC2 complex and for H3K27 methylation at its target genes in ESCs.

DISCUSSION

RBBP4 is a ubiquitously expressed nuclear protein that is a member of a highly conserved subfamily of WD repeat-containing proteins (Qian et al., 1993), and targeted disruption of *Rbbp4* leads to preimplantation embryonic lethality in mice (Miao et al., 2020), but the underlying molecular mechanisms are largely undetermined. Here, our data demonstrated that *Rbbp4* maintains the pluripotent and self-renewal state of ESCs by promoting transcription of pluripotency factors and repressing the expression of lineage-specific genes. We also show that *Rbbp4* targets the PRC2 complex to the promoters of lineage-specific genes to repress their expression in ESCs; thus, RBBP4 activity appears to be a key determinant of cell fate specification and lineage commitment in ESCs. Surprisingly, despite the striking similarity of the sequence shared by RBBP4 and RBBP7, and although both of them are often found within the same complexes, Rbbp4 but not Rbbp7 null mutants displayed severe defects, suggesting a specific role of Rbbp4 in sustaining ESC identity. The reason for such striking differences between Rbbp4 and Rbbp7 is not fully understood but it may be related to their chromatin binding ability in ESCs (Figure 7E).

RBBP4 tightly associates with EED, EZH1/2, and SUZ12 to form the core PRC2 complex

Although EZH1/2 catalyze H3K27me2/3, all the PRC2 core members are required for EZH1/2 to exert their catalytic activity. In addition, there are several substoichiometric accessory factors that associate with PRC2. In mammals, these include JARID2, AEBP2, PHF1, MTF2, and PHF19. Although these accessory components seem not particularly essential for PRC2 catalytic activity, they appear to modulate PRC2 enzymatic activity and/or its targeting to specific genomic loci. In this study, we demonstrated that *Rbbp4*-deficient ESCs, despite maintaining normal H3K27me3 levels, lost their normal undifferentiated colony morphologies and gave rise to flattened fibroblast-like cells. In addition, *Rbbp4*$^{\Delta/\Delta}$ cells failed to efficiently form colonies in secondary replating assays. Therefore, spontaneous differentiation induced by the ablation of *Rbbp4* in ESCs resulted in the loss of self-renewal and pluripotency. Apart from *Rbbp4*, no other PRC2 members has been shown to play an essential role in the maintenance of self-renewal of ESCs (Chamberlain et al., 2008). Importantly, concomitant disruption of *Ezh1/2*, *Eed*, and *Suz12* triggers spontaneous differentiation of ESCs toward primitive endoderm and mesoderm, a phenotype reminiscent

Figure 5. *Rbbp4* governs pluripotency by maintaining the expression of *Oct4* and *Sox2*

(A) Left: reference legend for cell lines used in Figure 5. Right: experimental diagrams of rescue assay.

(B) Representative images of the ESC colony of the indicated genotypes cultured for 7 days. Top, phase-contrast microscopy; bottom, AP staining.

(C) Percentage of isolated single ESCs of the indicated genotypes giving rise to macroscopic colonies.

(D) Bar graphs show the mean diameter of 30 random ESC colonies of the indicated genotypes.

(E) Quantitative analysis of colony formation assay in ESCs of indicated genotypes. AP-stained colonies were scored as undifferentiated (undiff.), mixed or differentiated (diff.).

(F) Western blot analysis of OCT4, SOX2, and NANOG protein levels after the overexpression of *Oct4*, *Sox2*, and *Nanog* in *Rbbp4*$^{F/F}$ ESCs and *Rbbp4*$^{\Delta/\Delta}$ ESCs.

(G) Time-course analysis of pluripotency-associated gene expression after expressing Cre in the corresponding cell lines by qRT-PCR.

Data in (C–E) represent the mean ± SD of three independent experiments. *$p < 0.05$, **$p < 0.01$, and ***$p < 0.001$ (Student's t test) compared with the control.

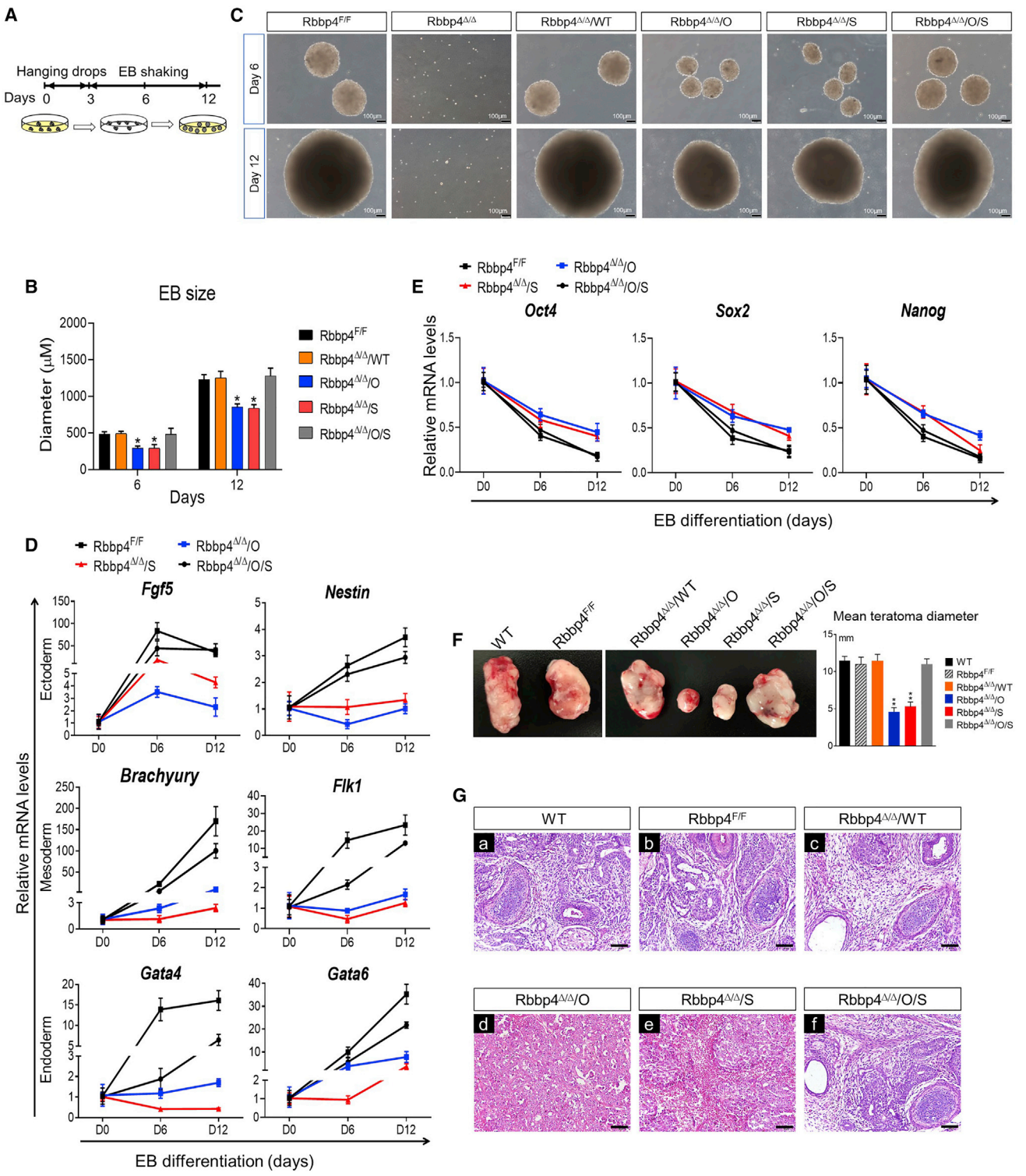

Figure 6. Overexpression of *Sox2* and *Oct4* maintains ESC self-renewal and pluripotency in the absence of *Rbbp4 in vitro* and *in vivo*

(A) Schematic illustration of the embryoid body (EB) formation procedure for differentiation of ESCs.

(B) The diameter statistics of EB. Thirty 30 EB diameters of each genotype were measured at each time point.

(C) Phase-contrast images of floating EB derived from indicated ESCs at day 6 and day 12. Scale bar, 100 μm.

(legend continued on next page)

of, but not as severe as, that seen in *Rbbp4*$^{\Delta/\Delta}$ ESCs. Notably, a considerable number of RBBP4 target regions was also occupied by EZH1/2, EED, and SUZ12, and was decorated with H3K27me3. These findings strongly implicate RBBP4 in recruitment of the PRC2 complex to target loci in ESCs. Indeed, EED, SUZ12, and EZH2, as well as the H3K27me3 mark, were absent or markedly reduced in *Rbbp4*$^{\Delta/\Delta}$ but not *Rbbp7*$^{\Delta/\Delta}$ ESCs. The most severe phenotype of *Rbbp4*$^{\Delta/\Delta}$ ESCs is accordance with the crucial importance of RBBP4 for genomic PRC2 targeting. As RBBP4 can associate with protein complexes other than PRC2 (Feng and Zhang, 2003; Kuzmichev et al., 2002), the severe phenotype in *Rbbp4*$^{\Delta/\Delta}$ ESCs can also be explained by the impaired function of these complexes in which RBBP4 is a common component. Notably, *Rbbp4* was previously identified as being essential for the maintenance of human ESCs (O'Connor et al., 2011). It will be interesting to see whether a similar mechanism also exists in human ESCs. Our study establishes a critical role of RBBP4 in the recruitment of the PRC2 complex to genes essential for ESC differentiation along the mesendoderm lineage. Dissecting the potential contribution of JARID2, AEBP2, PHF1, MTF2, and PHF19 to RBBP4-guided PRC2 chromatin occupancy is warranted for future investigation.

The maintenance of self-renewal and pluripotency of ESCs depends mostly on three core transcription factors namely SOX2, OCT4, and NANOG, which induce genes necessary for sustaining the undifferentiated state and repress others involved in lineage commitment and terminal differentiation (Loh et al., 2006; Young, 2011). Interestingly, these three master transcription factors jointly sustain each other's transcription in autoregulatory and feedforward loops in ESCs (Boyer et al., 2005). Here, we show that knockout of *Rbbp4* in ESCs dramatically reduces the expression of *Oct4*, *Sox2*, and *Nanog*. ChIP-seq and ChIP-qPCR demonstrated that the promoters of *Oct4* and *Sox2* were bound by RBBP4, suggesting that *Rbbp4* positively regulates their expression. *Oct4* and *Sox2* are of interest as they have been shown to be critical for the pluripotency and self-renewal of ESCs. Importantly, forced expression of *Oct4* or *Sox2* but not *Nanog* could partially rescue the defect in *Rbbp4*-deficient ESCs. In addition, the phenotypes in *Rbbp4*$^{\Delta/\Delta}$ ESCs could be fully rescued by co-overexpression of both *Oct4* and *Sox2*. However, several ChIP-seq studies have consistently failed to identify OCT4 and SOX2 as PRC2 target genes (Højfeldt et al., 2019; Tamburri et al., 2020), suggesting that Rbbp4 keeps the ESCs in a pluripotent state by maintaining the requisite levels of OCT4 and SOX2 in a PRC2-independent manner. In conclusion, our study strongly supports our model in which RBBP4 maintains ESCs in a pluripotent state by preventing mesendoderm specification and by regulating expression of Oct4 and Sox2 (Figure 7G).

RBBP4 was originally identified based on its interaction with the Rb tumor suppressor protein (Qian et al., 1993), which is essential for the maintenance of self-renewal and pluripotency in human ESCs (Chetty et al., 2013; Conklin et al., 2012; Conklin and Sage, 2009; Li et al., 2018b). The results of these studies in human ESCs together with our finding consolidate the notion that cell-cycle machinery and the maintenance of pluripotency are intricately connected to safeguard ESC identity (Pauklin and Vallier, 2013; Ruiz et al., 2011; Shcherbina et al., 2019). Interestingly, prevalent overexpression of Rbbp4 has been implicated in a variety of malignancies (Li et al., 2018a), suggesting that induction of carcinoma cell differentiation by directly targeting Rbbp4 might be a promising therapeutic approach for tumor treatment.

EXPERIMENTAL PROCEDURES

CRISPR-Cas9-mediated genome editing

The pSptCas9(BB)-2A-Puro(PX459) V2.0 vector was obtained from Addgene (no. 62988) and sgRNAs were designed using online CRISPR design tool (http://crispor.tefor.net). To generate stable knockout ESC lines, ESCs were transfected with a pair of Cas9 guides flanking the deletion region using Lipofectamine 2000 according to the manufacturer's instruction. Genomic DNA samples from individual ESC clones were PCR screened for the desired deletion and correct clones were validated by both qRT-PCR and western blot. To generate a conditional knockout of Rbbp4 in ESCs, ESCs were subjected to genomic engineering to flank the third

(D) qRT-PCR analysis of lineage-specific markers at day 0, day 6, and day 12 during EB formation from the indicated ESC lines. *Fgf5*, *Nestin* (ectoderm), *Brachyury*, *Flk1* (mesoderm), and *Gata4*, *Gata6* (endoderm). Data are normalized to the expression levels in ESCs. Error bars represent ± SD (n = 3).

(E) qRT-PCR mRNA analysis of pluripotency markers during time-course differentiation of *Rbbp4*$^{F/F}$, and rescue of *Rbbp4* in *Rbbp4*$^{\Delta/\Delta}$ EBs. Samples were collected at different days.

(F) *In vivo* differentiation potential of formation teratomas of indicated ESCs. Left: the morphological characteristics of teratomas are shown. Right: average teratoma size at 4 weeks after injection in the indicated groups.

(G) Histological analysis of teratomas. (A–F) Histological sections of hematoxylin and eosin-stained teratomas. (A, B, C, F) Each teratoma contained three embryonic germ layer tissues. (D and E) Immature germ layer differentiation is shown. Scale bar, 50 μm.

Data in (B and D–F) represent mean ± SD obtained from three independent experiments. *p < 0.05 and **p < 0.01 (Student's t test) compared with the control.

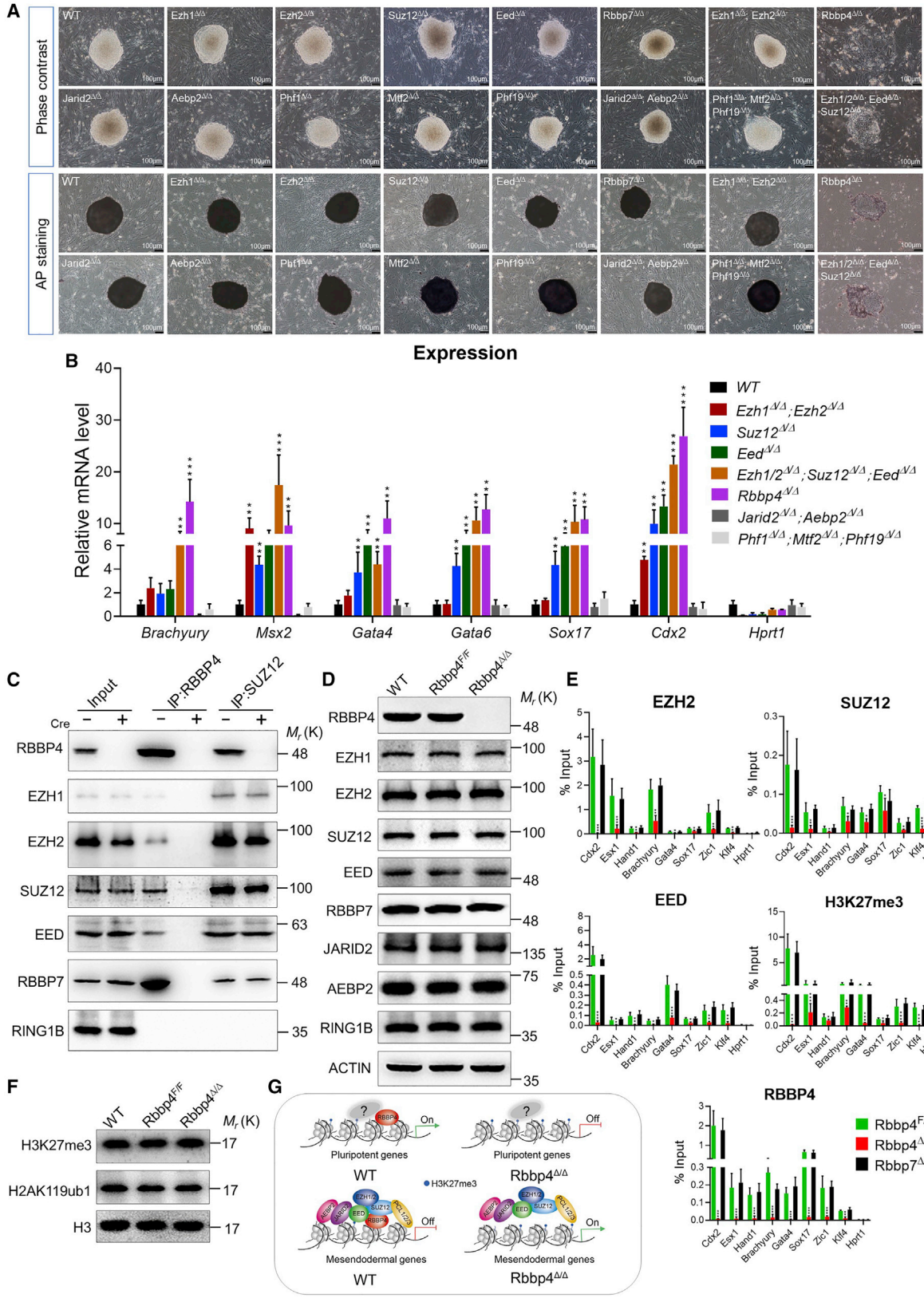

(legend on next page)

coding exon of *Rbbp4* (exon 3) with *loxP* sites in a parallel orientation using homology arms of approximately 2 kb and appropriate Cas9 guides. Correct $Rbbp4^{F/F}$ clones were validated by both qRT-PCR and western blot to confirm Rbbp4 removal by transient transfection of a Cre-expressing plasmid.

Statistics

Statistical analysis was carried out using GraphPad Prism 8.0 software. All experiments were carried out in at least three independent biological replicates for each group unless stated otherwise. All data are expressed as mean ± SD. Statistical significance is presented in the figures as *p < 0.05, **p < 0.01, ***p < 0.001, and not significant (ns, p > 0.05) (Student's t test).

Data and code availability

Sequencing data performed for this study are deposited in GEO database under the accession numbers GSE144155 (RNA-seq) and GSE155029 (ChIP-seq). Additional datasets used in this study are detailed in Table S4.

SUPPLEMENTAL INFORMATION

Supplemental information can be found online at https://doi.org/10.1016/j.stemcr.2021.01.009.

AUTHOR CONTRIBUTIONS

Conceptualization, J.Q.; methodology, T.S., C.W., S.L., Y.Z., and K.H.; formal analysis, C.W., T.S., Y.Z., L.D., and J.Q.; mechanistic investigations, C.W., S.L., L.D., Y.Z., Y.H., and J.Q.; writing – original draft, Y.H. and J.Q.; writing – review & editing, J.Q., Y.H., Y.X., and Q.J.; funding acquisition, J.Q.; supervision, J.Q.

ACKNOWLEDGMENTS

We are indebted to Drs Zhenji Gan and Lin Liu for their helpful suggestions and for kindly providing reagents. We thank members of our laboratory for helpful discussion. This work was supported by grants from the National Natural Science Foundation of China (31970810 and 31671532) to J.Q.

Received: August 1, 2020
Revised: January 16, 2021
Accepted: January 19, 2021
Published: February 18, 2021

REFERENCES

Blackledge, N.P., Farcas, A.M., Kondo, T., King, H.W., McGouran, J.F., Hanssen, L.L., Ito, S., Cooper, S., Kondo, K., Koseki, Y., et al. (2014). Variant PRC1 complex-dependent H2A ubiquitylation drives PRC2 recruitment and polycomb domain formation. Cell *157*, 1445–1459.

Boyer, L.A., Lee, T.I., Cole, M.F., Johnstone, S.E., Levine, S.S., Zucker, J.P., Guenther, M.G., Kumar, R.M., Murray, H.L., Jenner, R.G., et al. (2005). Core transcriptional regulatory circuitry in human embryonic stem cells. Cell *122*, 947–956.

Chamberlain, S.J., Yee, D., and Magnuson, T. (2008). Polycomb repressive complex 2 is dispensable for maintenance of embryonic stem cell pluripotency. Stem Cells *26*, 1496–1505.

Chetty, S., Pagliuca, F.W., Honore, C., Kweudjeu, A., Rezania, A., and Melton, D.A. (2013). A simple tool to improve pluripotent stem cell differentiation. Nat. Methods *10*, 553–556.

Conklin, J.F., Baker, J., and Sage, J. (2012). The RB family is required for the self-renewal and survival of human embryonic stem cells. Nat. Commun. *3*, 1244.

Conklin, J.F., and Sage, J. (2009). Keeping an eye on retinoblastoma control of human embryonic stem cells. J. Cell. Biochem. *108*, 1023–1030.

Conway, E., Jerman, E., Healy, E., Ito, S., Holoch, D., Oliviero, G., Deevy, O., Glancy, E., Fitzpatrick, D.J., Mucha, M., et al. (2018). A family of vertebrate-specific polycombs encoded by the LCOR/LCORL genes balance PRC2 subtype activities. Mol. Cell *70*, 408–421 e408.

Das, P.P., Hendrix, D.A., Apostolou, E., Buchner, A.H., Canver, M.C., Beyaz, S., Ljuboja, D., Kuintzle, R., Kim, W., Karnik, R., et al. (2015). PRC2 is required to maintain expression of the maternal Gtl2-rian-Mirg locus by preventing de novo DNA methylation in mouse embryonic stem cells. Cell Rep. *12*, 1456–1470.

Figure 7. RBBP4 guides PRC2 recruitment and H3K27 trimethylation at genomic loci

(A) Bright-field images of an ESC colony of wild-type and indicated genotypes after 7 days of culture. AP staining images of the ESC colony that arose from the wild-type and indicated genotypes. Scale bar, 100 μm.

(B) qRT-PCR quantification of *Rbbp4* targets in indicated cell lines normalized to β-actin. *Hprt1* is represented as a negative control.

(C) Endogenous coimmunoprecipitations of RBBP4 and SUZ12 in $Rbbp4^{F/F}$ transfected with Cre (+) or control vector (−) for 72 h, followed by western blot analysis with the indicated antibodies against core subunits of PRC2.

(D) Western blot analyses using the indicated antibodies against PRC2 subunits on whole-cell lysates from wild-type (WT), $Rbbp4^{F/F}$, and $Rbbp4^{\Delta/\Delta}$ ESCs.

(E) ChIP-qPCR analysis of EZH2, SUZ12, EED, H3K27me3, and RBBP4 binding at the indicated regions of pluripotent transcription factors and mesendodermal genes (normalized to input) in $Rbbp4^{F/F}$, $Rbbp7^{\Delta/\Delta}$, or $Rbbp4^{F/F}$ ESCs that were transfected with Cre after 3 days.

(F) Western blot for H3K27 tri-methylation and H2AK119 mono-ubiquitination on nuclear lysates from $Rbbp4^{\Delta/\Delta}$ and matched control ESCs. Histone 3 was used as a loading control.

(G) Proposed model of Rbbp4-mediated pluripotency maintenance of ESCs.

Data in (B and E) represent the mean ± SD of three independent experiments. *p < 0.05, **p < 0.01, and ***p < 0.001 (Student's t test) compared with the control. See also Figures S5 and S6.

Di Croce, L., and Helin, K. (2013). Transcriptional regulation by Polycomb group proteins. Nat. Struct. Mol. Biol. *20*, 1147–1155.

Ding, J., Huang, X., Shao, N., Zhou, H., Lee, D.F., Faiola, F., Fidalgo, M., Guallar, D., Saunders, A., Shliaha, P.V., et al. (2015). Tex10 coordinates epigenetic control of super-enhancer activity in pluripotency and reprogramming. Cell Stem Cell *16*, 653–668.

Faust, C., Lawson, K.A., Schork, N.J., Thiel, B., and Magnuson, T. (1998). The Polycomb-group gene eed is required for normal morphogenetic movements during gastrulation in the mouse embryo. Development *125*, 4495–4506.

Feng, Q., and Zhang, Y. (2003). The NuRD complex: linking histone modification to nucleosome remodeling. Curr. Top. Microbiol. Immunol. *274*, 269–290.

Højfeldt, J.W., Hedehus, L., Laugesen, A., Tatar, T., Wiehle, L., and Helin, K. (2019). Non-core subunits of the PRC2 complex are collectively required for its target-site specificity. Mol. Cell *76*, 423–436.e423.

Holoch, D., and Margueron, R. (2017). Mechanisms regulating PRC2 recruitment and enzymatic activity. Trends Biochem. Sci. *42*, 531–542.

Kuroda, M.I., Kang, H., De, S., and Kassis, J.A. (2020). Dynamic competition of polycomb and trithorax in transcriptional programming. Annu. Rev. Biochem. *89*, 235–253.

Kuzmichev, A., Zhang, Y., Erdjument-Bromage, H., Tempst, P., and Reinberg, D. (2002). Role of the Sin3-histone deacetylase complex in growth regulation by the candidate tumor suppressor p33(ING1). Mol. Cell. Biol. *22*, 835–848.

Li, D., Song, H., Mei, H., Fang, E., Wang, X., Yang, F., Li, H., Chen, Y., Huang, K., Zheng, L., et al. (2018a). Armadillo repeat containing 12 promotes neuroblastoma progression through interaction with retinoblastoma binding protein 4. Nat. Commun. *9*, 2829.

Li, J., Narayanan, C., Bian, J., Sambo, D., Brickler, T., Zhang, W., and Chetty, S. (2018b). A transient DMSO treatment increases the differentiation potential of human pluripotent stem cells through the Rb family. PLoS one *13*, e0208110.

Loh, Y.H., Wu, Q., Chew, J.L., Vega, V.B., Zhang, W., Chen, X., Bourque, G., George, J., Leong, B., Liu, J., et al. (2006). The Oct4 and Nanog transcription network regulates pluripotency in mouse embryonic stem cells. Nat. Genet. *38*, 431–440.

Margueron, R., Li, G., Sarma, K., Blais, A., Zavadil, J., Woodcock, C.L., Dynlacht, B.D., and Reinberg, D. (2008). Ezh1 and Ezh2 maintain repressive chromatin through different mechanisms. Mol. Cell *32*, 503–518.

Miao, X., Sun, T., Barletta, H., Mager, J., and Cui, W. (2020). Loss of RBBP4 results in defective inner cell mass, severe apoptosis, hyperacetylated histones and preimplantation lethality in mice. Biol. Reprod. *103*, 13–23.

Montgomery, N.D., Yee, D., Chen, A., Kalantry, S., Chamberlain, S.J., Otte, A.P., and Magnuson, T. (2005). The murine polycomb group protein Eed is required for global histone H3 lysine-27 methylation. Curr. Biol. *15*, 942–947.

O'Carroll, D., Erhardt, S., Pagani, M., Barton, S.C., Surani, M.A., and Jenuwein, T. (2001). The polycomb-group gene Ezh2 is required for early mouse development. Mol. Cell. Biol. *21*, 4330–4336.

O'Connor, M.D., Wederell, E., Robertson, G., Delaney, A., Morozova, O., Poon, S.S., Yap, D., Fee, J., Zhao, Y., McDonald, H., et al. (2011). Retinoblastoma-binding proteins 4 and 9 are important for human pluripotent stem cell maintenance. Exp. Hematol. *39*, 866–879.e861.

Pasini, D., Bracken, A.P., Hansen, J.B., Capillo, M., and Helin, K. (2007). The polycomb group protein Suz12 is required for embryonic stem cell differentiation. Mol. Cell. Biol. *27*, 3769–3779.

Pasini, D., Bracken, A.P., Jensen, M.R., Lazzerini Denchi, E., and Helin, K. (2004). Suz12 is essential for mouse development and for EZH2 histone methyltransferase activity. EMBO J. *23*, 4061–4071.

Pauklin, S., and Vallier, L. (2013). The cell-cycle state of stem cells determines cell fate propensity. Cell *155*, 135–147.

Pereira, C.F., Piccolo, F.M., Tsubouchi, T., Sauer, S., Ryan, N.K., Bruno, L., Landeira, D., Santos, J., Banito, A., Gil, J., et al. (2010a). ESCs require PRC2 to direct the successful reprogramming of differentiated cells toward pluripotency. Cell Stem Cell *6*, 547–556.

Pereira, J.D., Sansom, S.N., Smith, J., Dobenecker, M.W., Tarakhovsky, A., and Livesey, F.J. (2010b). Ezh2, the histone methyltransferase of PRC2, regulates the balance between self-renewal and differentiation in the cerebral cortex. Proc. Natl. Acad. Sci. U S A *107*, 15957–15962.

Piunti, A., and Shilatifard, A. (2016). Epigenetic balance of gene expression by Polycomb and COMPASS families. Science *352*, aad9780.

Qian, Y.W., Wang, Y.C., Hollingsworth, R.E., Jr., Jones, D., Ling, N., and Lee, E.Y. (1993). A retinoblastoma-binding protein related to a negative regulator of Ras in yeast. Nature *364*, 648–652.

Ruiz, S., Panopoulos, A.D., Herrerías, A., Bissig, K.D., Lutz, M., Berggren, W.T., Verma, I.M., and Izpisua Belmonte, J.C. (2011). A high proliferation rate is required for cell reprogramming and maintenance of human embryonic stem cell identity. Curr. Biol. *21*, 45–52.

Schuettengruber, B., Bourbon, H.M., Di Croce, L., and Cavalli, G. (2017). Genome regulation by polycomb and trithorax: 70 years and counting. Cell *171*, 34–57.

Shcherbina, A., Li, J., Narayanan, C., Greenleaf, W., Kundaje, A., and Chetty, S. (2019). Brief report: cell cycle dynamics of human pluripotent stem cells primed for differentiation. Stem Cells *37*, 1151–1157.

Simon, J.A., and Kingston, R.E. (2009). Mechanisms of polycomb gene silencing: knowns and unknowns. Nat. Rev. Mol. Cel. Biol. *10*, 697–708.

Tamburri, S., Lavarone, E., Fernández-Pérez, D., Conway, E., Zanotti, M., Manganaro, D., and Pasini, D. (2020). Histone H2AK119 mono-ubiquitination is essential for polycomb-mediated transcriptional repression. Mol. Cell *77*, 840–856.e845.

Turner, S.A., and Bracken, A.P. (2013). A "complex" issue: deciphering the role of variant PRC1 in ESCs. Cell Stem Cell *12*, 145–146.

Young, R.A. (2011). Control of the embryonic stem cell state. Cell *144*, 940–954.

Zhou, Y., Zhou, B., Pache, L., Chang, M., Khodabakhshi, A.H., Tanaseichuk, O., Benner, C., and Chanda, S.K. (2019). Metascape provides a biologist-oriented resource for the analysis of systems-level datasets. Nat. Commun. *10*, 1523.

Stem Cell Reports, Volume *16*

Supplemental Information

Rbbp4 Suppresses Premature Differentiation of Embryonic Stem Cells

Yikai Huang, Ting Su, Congcong Wang, Lixia Dong, Shuang Liu, Yaru Zhu, Kunying Hao, Yin Xia, Qing Jiang, and Jinzhong Qin

Supplemental Information

Rbbp4 Suppresses Premature Differentiation of Embryonic Stem Cells

Yikai Huang, Ting Su, Congcong Wang, Lixia Dong, Shuang Liu, Yaru Zhu, Kunying Hao, Yin Xia, Qing Jiang, Jinzhong Qin

Supplemental Figures and Legends

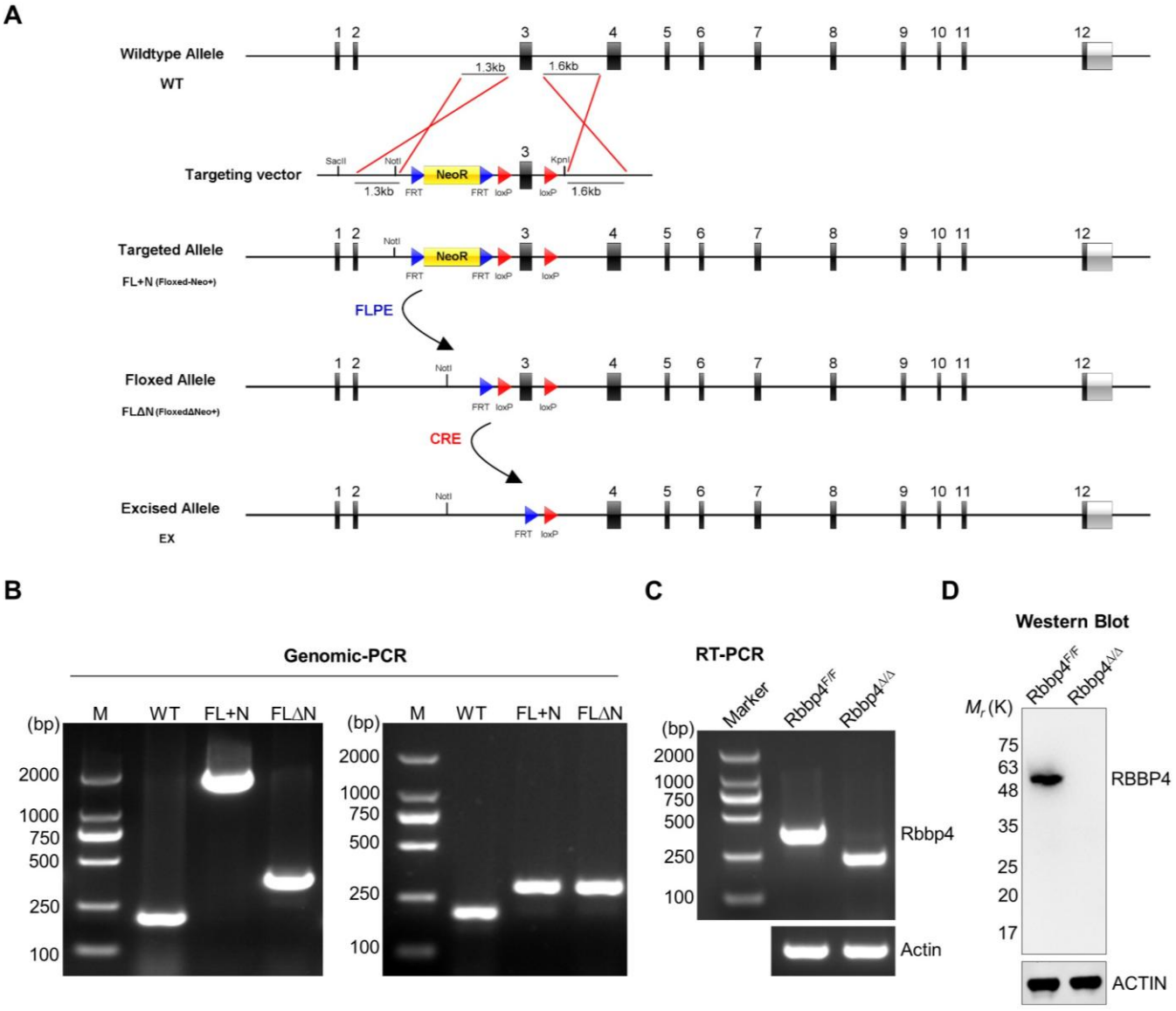

Figure S1. Generation of Conditional Inactivation of *Rbbp4* in ESCs, Related to Figure 1

(A) Overview of the gene targeting strategy. The wildtype *Rbbp4* locus, *Rbbp4* gene-targeting vector, the targeted allele and the excised allele are shown. (B) Genomic PCR analysis of the targeted allele and the floxed allele. (C) RT-PCR analysis for residual *Rbbp4* mRNA revealing a shorter band by transient expression of Cre recombinase. (D) Western blot analysis using a specific antibody against RBBP4 demonstrating absence of the protein in the sample three days after transient expression of Cre. ACTIN served as a loading control.

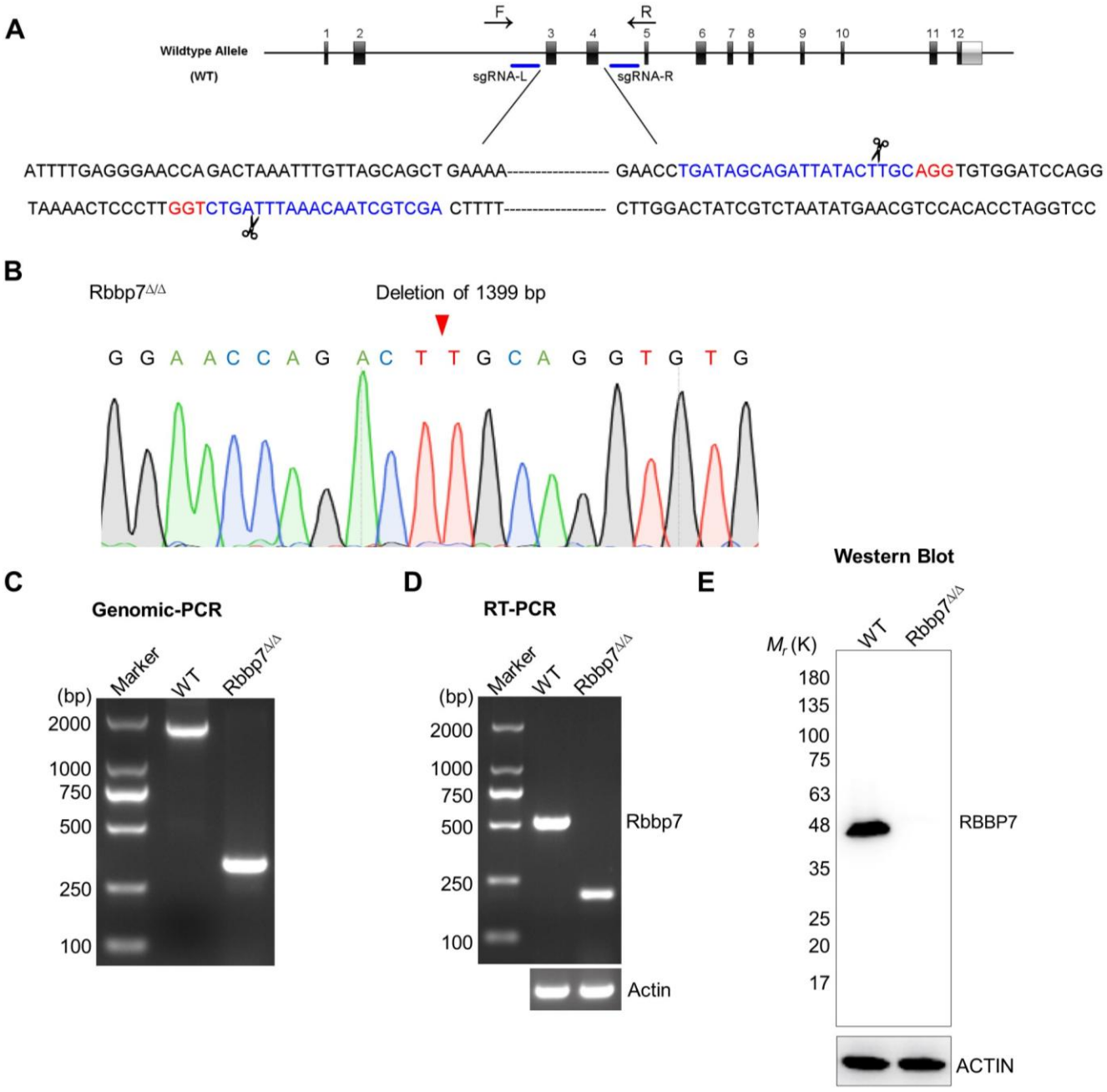

Figure S2. Generation of *Rbbp7* Null ESCs by CRISPR-Cas9, Related to Figure 1

(A) Schematic illustration for production of *Rbbp7* knockout ESCs via CRISPR/Cas9-mediated gene targeting. The sgRNA sequences are highlighted in blue and PAM sequences are in red. Primers used for PCR and sequencing are depicted as gray arrows. (B) Direct sequencing of the PCR product from *Rbbp7*$^{\Delta/\Delta}$ ESCs determining deletion of 1399bp DNA fragment. (C) Genotyping of *Rbbp7*$^{\Delta/\Delta}$ ESCs using primers on the both sides of targeted region. (D) RT-PCR analysis of *Rbbp7*$^{\Delta/\Delta}$ ESCs showing a shorter band in the mutant. *β-actin* was shown as a loading control. (E) Western blot analysis revealing the absence of RBBP7 protein in *Rbbp7*$^{\Delta/\Delta}$ ESCs. ACTIN was shown as a loading control.

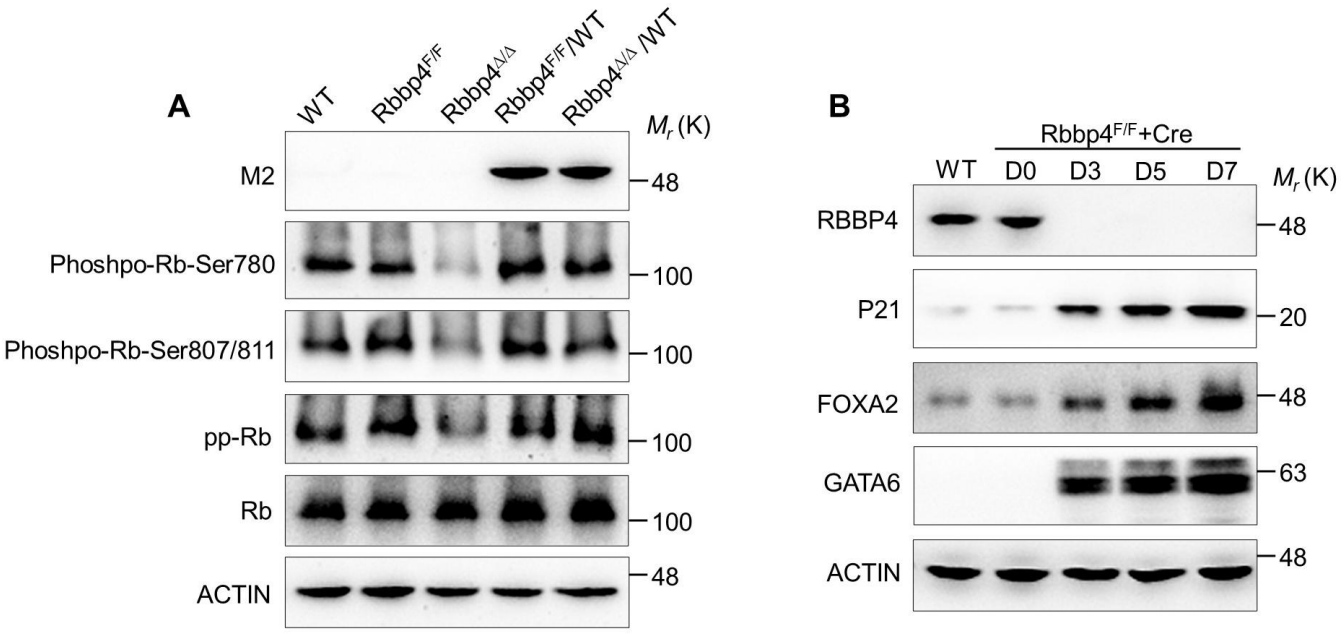

Figure S3. Loss of *Rbbp4* resulting in reduced levels of the phosphorylated and hyperphosphorylated forms of the Rb protein (ppRb), Related to Figures 1 and 2

(A) Western blot analysis of the phosphorylated and hyperphosphorylated forms of the Rb protein in ESCs of the indicated genotypes. (B) Western blot for P21, FOXA2 and GATA6 in *Rbbp4*$^{F/F}$ following transfection with Cre. ACTIN was used as a loading control.

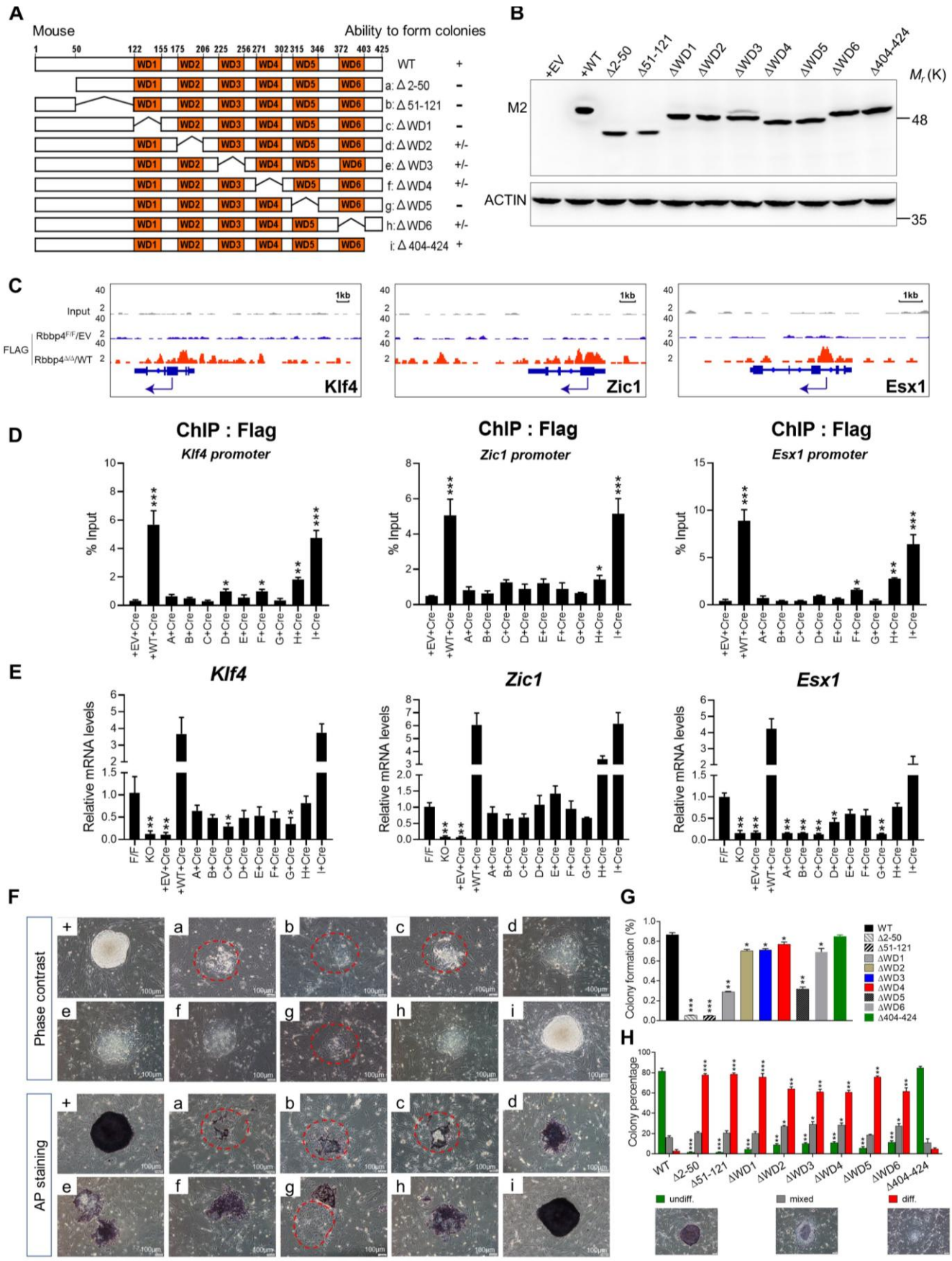
A
Mouse
Ability to form colonies
WT +
a: Δ 2-50 -
b: Δ 51-121 -
c: ΔWD1 -
d: ΔWD2 +/-
e: ΔWD3 +/-
f: ΔWD4 +/-
g: ΔWD5 -
h: ΔWD6 +/-
i: Δ 404-424 +
B
+EV
+WT
Δ2-50
Δ51-121
ΔWD1
ΔWD2
ΔWD3
ΔWD4
ΔWD5
ΔWD6
Δ404-424
Mr (K)
M2
ACTIN
48
35
C
Input
FLAG
Rbbp4F/F/EV
Rbbp4Δ/Δ/WT
1kb
Klf4
Zic1
Esx1
D
ChIP : Flag
Klf4 promoter
Zic1 promoter
Esx1 promoter
% Input
+EV+Cre
+WT+Cre
A+Cre
B+Cre
C+Cre
D+Cre
E+Cre
F+Cre
G+Cre
H+Cre
I+Cre
E
Klf4
Zic1
Esx1
Relative mRNA levels
F/F
KO
+EV+Cre
+WT+Cre
F
Phase contrast
AP staining
G
Colony formation (%)
WT
Δ2-50
Δ51-121
ΔWD1
ΔWD2
ΔWD3
ΔWD4
ΔWD5
ΔWD6
Δ404-424
H
Colony percentage
undiff.
mixed
diff.

Figure S4. Schematic domain structures and function analysis of Rbbp4 and its deletion mutants, Related to Figure 3

(A) Schematic domain structures and function analysis of RBBP4 and its deletion mutants. A concise schematic diagram of known structural characteristics of wild-type RBBP4 is shown at the top of the panel. The thin broken lines represent deleted regions. Results of pluripotency rescue assays using *Rbbp4*$^{F/F}$ ESCs reexpressing wild-type RBBP4 or deletion mutant proteins are presented on the right. +, rescue; +/–, partial rescue; –, no rescue. (B) The expression of different *Rbbp4* deletion mutant proteins in *Rbbp4* null ESCs. Protein levels of corresponding RBBP4 mutants were examined by western blotting with anti-FLAG antibody. ACTIN served as the loading control. (C) RBBP4 peaks at the indicated pluriptency-associated gene locus. (D) ChIP-qPCR analysis of RBBP4 binding to the select promoter regions in wild-type and deletion mutants. (E) Real-time PCR detecting *Klf4*, *Esx1*, and *Zic1* expression levels in indicated ESCs reexpressed wild-type and deletion mutants. Data were normalized to *β-actin* and values are represented as mean ± SD, (n=3). (F) Summary of results from rescue of *Rbbp4* deletion mutants. Morphology of respective mutant ESC colony with (bottom) or without (top) AP staining. The outlines of obviously defective colonies are circled. Scale bar, 100μm. (G) Percentage of isolated single ESCs of the indicated genotypes giving rise to macroscopic colonies. (H) Quantitative analysis of colony formation assay in ESCs of indicated genotypes. AP-stained colonies were scored as undifferentiated (undiff.), mixed or differentiated (diff.). Data are plotted as mean ± SD of three independent experiments in triplicates. *$p < 0.05$, **$p < 0.01$ and ***$p < 0.001$ (Student's t test) compared with the control.

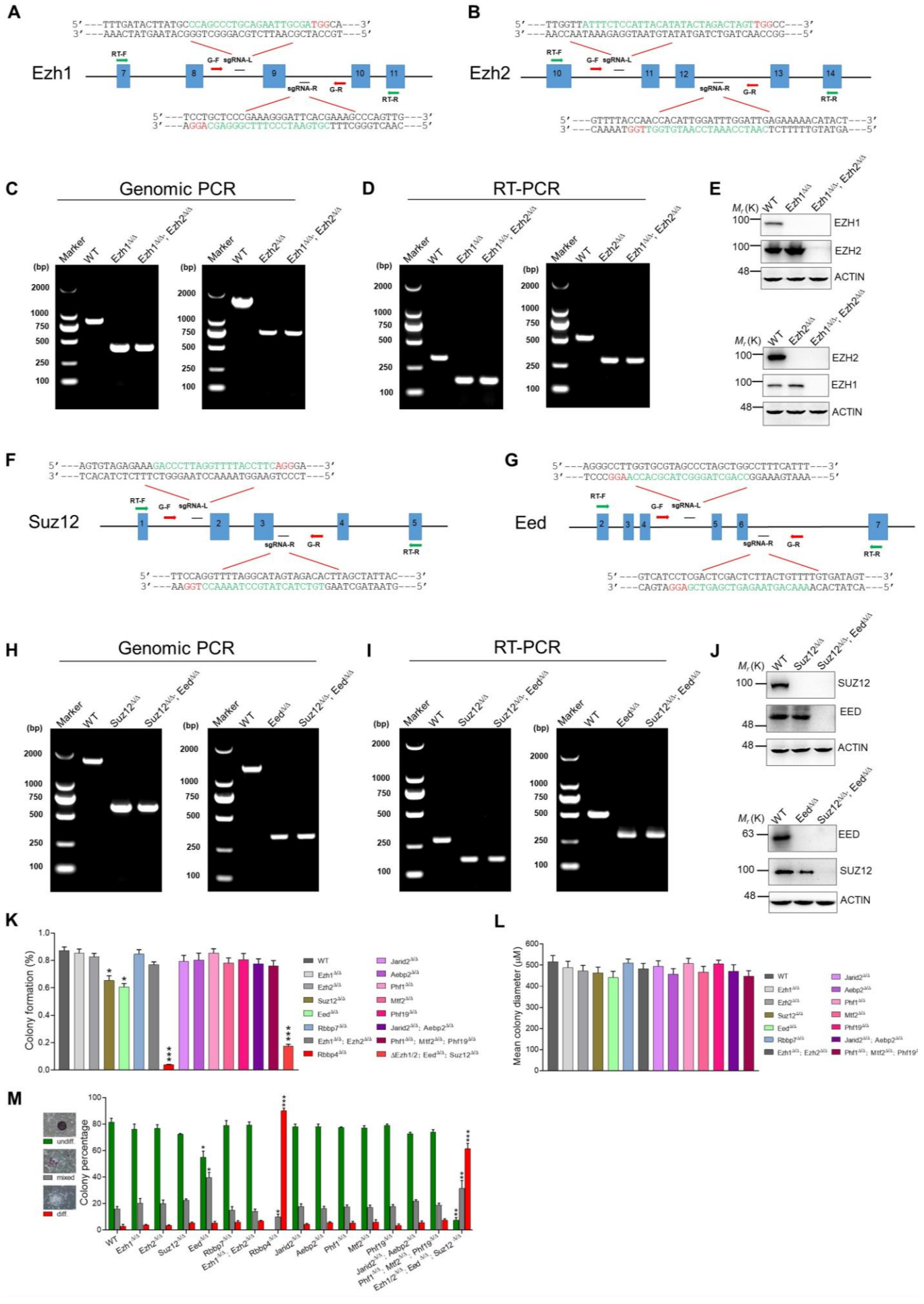
A
Ezh1
RT-F
G-F
sgRNA-L
sgRNA-R
G-R
RT-R
B
Ezh2
C
Genomic PCR
Marker
WT
Ezh1Δ/Δ
Ezh1Δ/Δ; Ezh2Δ/Δ
Ezh2Δ/Δ
(bp)
D
RT-PCR
E
Mr(K)
EZH1
EZH2
ACTIN
F
Suz12
G
Eed
H
Genomic PCR
Suz12Δ/Δ
Suz12Δ/Δ; EedΔ/Δ
EedΔ/Δ
I
RT-PCR
J
SUZ12
EED
K
Colony formation (%)
L
Mean colony diameter (μM)
M
Colony percentage
undiff.
mixed
diff.

Figure S5. Generation of Single Knockout and Combined Knockout ESC lines of PRC2 Core Subunits, Related to Figure 7

(A, B, F, G) Schematic overview of the strategy to generate *Ezh1*, *Ezh2*, *Suz12* and *Eed* knockout ESCs, respectively. PAM sequences are in red following the sgRNA sequence highlighted in green. The locations of genomic PCR primers (G-F, Forward; G-R, Reverse) are indicated by red arrows. (C, H) Genotyping of indicated knockout ESCs using primers upstream and downstream of the deleted region. (D, I) RT-PCR analysis for residual mRNAs revealing a shorter band in corresponding mutants. RT-PCR primers were represented by green arrows. *β-actin* served as a loading control. (E, J) Western blot analysis using specific antibodies recognizing related proteins demonstrating absence of the protein in knockout ESC lines. (K) Percentage of isolated single ESCs of the indicated genotypes giving rise to colonies. (L) Bar graphs summarize the mean diameter of 30 random ESC colonies of the indicated genotypes. (M) Quantitative analysis of colony formation assay in ESCs of indicated genotypes. AP-stained colonies were scored as undifferentiated (undiff.), mixed or differentiated (diff.). Data in (K) to (M) represent as mean ± SD obtained from three independent experiments, $*p < 0.05$, $**p < 0.01$ and $***p < 0.001$ (Student's t test) compared with the control.

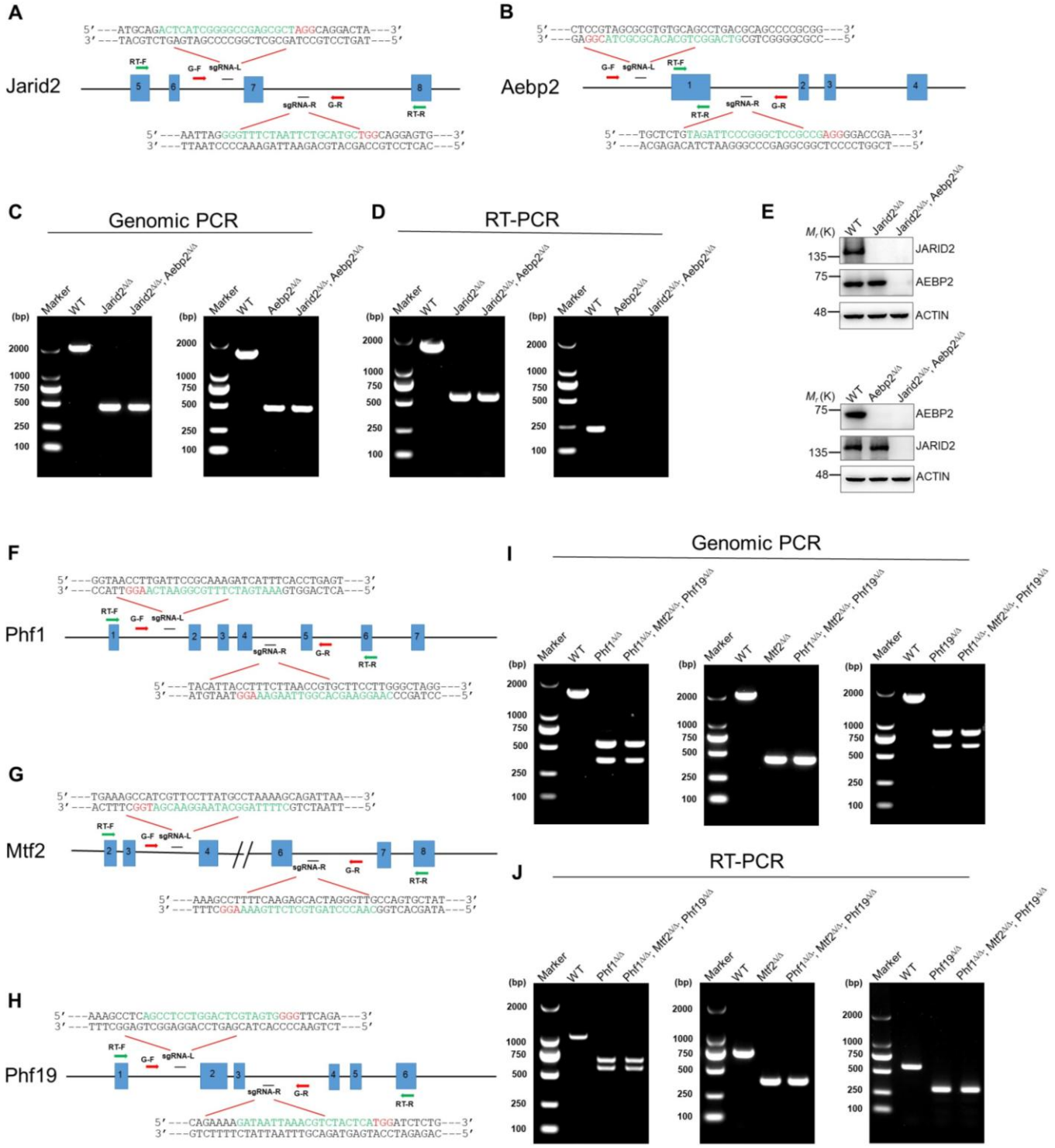

Figure S6. Generation of *Jarid2*, *Aebp2* or *Pcl1-3* Knockout ESCs, Related to Figure 7

(A, B, F, G, H) The schematic of *Jarid2*, *Aebp2* and *Pcl1-3* gene targeting strategies, respectively. Deleted regions are shown on the corresponding panels. The locations of genomic PCR primers (G-F, Forward; G-R, Reverse) are shown by red arrows, and RT-PCR primers (RT-F, Forward; RT-R, Reverse) are represented by green arrows. (C, I) Genomic PCR for analysis of indicated knockout ESCs. (D) RT-PCR analysis for residual *Jarid2*, *Aebp2* and *Pcl1-3* mRNA. (E) The absence of the proteins JARID2 or AEBP2 in knockout ESCs analyzed by Western blot. ACTIN served as a loading control.

Supplemental Tables

Table S1. All sgRNA sequences and primer sequences for genomic PCR and RT-PCR used in this study.

SgRNAs (related to Figures. 1, 7 and S1, S2, S5 and S6)		
Gene Name	**Upstream sgRNA**	**Downstream sgRNA**
Rbbp4	GTGATGACTAATTGTCCTCT	GGCCCAGGTTCAATTCCCAA
Rbbp7	AGATGGGAAGCAGGGTTTTG	TGATAGCAGATTATACTTGC
Ezh1	CCAGCCCTGCAGAATTGCGA	CGTGAATCCCTTTCGGGAGC
Ezh2	ATTACATATACTAGACTAGT	CAATCCAAATCCAATGTGGT
Suz12	GACCCTTAGGTTTTACCTTC	TGTCTACTATGCCTAAAACC
Eed	CCAGCTAGGGCTACGCACCA	AAACAGTAAGAGTCGAGTCG
Jarid2	ACTCATCGGGGCCGAGCGCT	GGGTTTCTAATTCTGCATGC
Aebp2	GTCAGGCTGCACACGCGCTA	TAGATTCCCGGGCTCCGCCG
Phf1	AAATGATCTTTGCGGAATCA	CAAGGAAGCACGGTTAAGAA
Mtf2	CTTTTAGGCATAAGGAACGA	CAACCCTAGTGCTCTTGAAA
Phf19	AGCCTCCTGGACTCGTAGTG	GATAATTAAACGTCTACTCA
Pou5f1	GGATTACATGCTCGTTCGTC	TACTGGCTTTCTCCAACCGC
Primers_Genomic PCR (related to Figures. S1, S2, S5 and S6)		
Gene Name	**5' Forward**	**5' Reverse**
Rbbp4	GGATCCCTCAGTCTCACCAG	TCCTGCCTCATGTGCCTTAG
Rbbp7	AGATGGGAAGCAGGGTTTTG	TCATTGTTGAAGCTGCTGGT
Ezh1	CTGCTTTTGAGGACGTCTGG	TTGACTGGAGTGAGCAGAGG
Ezh2	GTACCCTCTTCCCCTGTTCC	ACACAGTGGGTTGAGGTAGG
Suz12	TGGCGTAAATGTGTGTGTGG	CGCGCGTGTTCTCATCTTTA
Eed	AGGGTGACACTGAATCTGCA	CTCTCTCCTGCCACCTACAC
Jarid2	AGTGTGCTGGGTTCTTGCTT	AACCCTAAAACCCCAGGATG
Aebp2	CTTGCTCCACTTACGGCTTC	CTTGCTCCACTTACGGCTTC
Phf1	GGGGCACTCAGGGAAGTTAT	TGCAGAGGGACAGACAGATG
Mtf2	AGTGACGCTGGGTCTTGTCT	ACACTCCAAAGTGGCAAAGG
Phf19	GGGGAGAGCCAGATGTGTTA	ATGGCCACTTTCATGCTTTC
Primers_RT-PCR (related to Figures. S1, S2, S5 and S6)		
Gene Name	**5' Forward**	**5' Reverse**
Rbbp4	GGAAGAACGGGTGATCAACG	AGGGGTTCTGAGGCATGTAC
Rbbp7	TTCAGTGGCCCAGTCTTACC	TTTGCCTTCCTTTGGTCCTG
Ezh1	CCATTGCGTCCATGTTTCCT	CATGGCGTACTCCTTTGCTC
Ezh2	AAAGACACCACCTAAACGCC	ACATGGTTAGAGGAGCCGTC
Suz12	AGAAGCCGAAAATGGAGCAC	TGTGGAAGAAACCGGTAAATGT
Eed	AGGAAGGAAAAGCTGGGGAA	CCCTTCCACACCTCCGAATA
Jarid2	CTTCATCTTCGTGCCAGTCA	CAGGGAGTGGAACTTGTGGT
Aebp2	GACGAGGACGAGGAGGAC	CACGCTACTGCTGCTGCTAC
Phf1	CCTTCTGTCGACTCCTCCTG	TTACAGCAAACGCTGAGGTG
Mtf2	CAAGCGGTCTCCTTTACGTC	TGGTCCAGAACTGCAGACAG
Phf19	CAAGTGGGACCGGCTGAC	GCTGGTAGGACAGCACCATT

Table S2. All primer sequences for RT-qPCR and ChIP-qPCR used in this study.

Primers_RT-qPCR (related to Figures. 2, 4, 5, 6 and 7)		
Gene Name	**5' Forward**	**5' Reverse**
Dppa5a	CAGGCCATGTTTGAGCTGAA	ACTCGATACACTGGCCTAGC
Fgf4	TCTGCCCAACAACTACAACG	GAGGGGTAGGGTGTGCTTC
Lefty1	CGCACTGCCCTTATCGATTC	ACTTGTGTGAGCTCCAGGTT
Nanog	ATGCGGACTGTGTTCTCTCA	CCGCTTGCACTTCATCCTTT
Utf1	AGACTCTGCCTACTTACCGC	TCTGGTTATCGAAGGGTCCG
Foxd3	CGAGTTCATCAGCAACCGTT	GGTCCAGGGTCCAGTAGTTG
Tcl1	TTTCCTCTACACTGGGCTCC	GAGGAGGTGAGGAGAACTGG
Sox2	CGCGGAGTGGAAACTTTTGT	CGGGAAGCGTGTACTTATCC
Pou5f1	GGATGGCATACTGTGGACCT	TCTCCAACTTCACGGCATTG
Nr5a2	TGAAGCAGCAGAAGAAAGCC	TGTCATAGTCTGTCGGAGGC
Sox17	GCCGAGCCAAAGCGG	GTCAACGCCTTCCAAGACTTG
Fgf5	TTGCGACCCAGGAGCTTAAT	CTACGCCTCTTTATTGCAGC
Brachyury	CCAAGGACAGAGAGACGGCT	AGTAGGCATGTTCCAAGGGC
Flk1	GCTTGCTCCTTCCTCATCTC	CCATCAGGAAGCCACAAAGC
Gata6	CCCACTTCTGTGTTCCCAATTG	TTGGTCACGTGGTACAGGCG
Foxa2	CCCTACGCCAACATGAACTCG	GTTCTGCCGGTAGAAAGGGA
Sox11	AGAACATCACCAAGCAGCAG	TCCTTATCCACCAGCGACAG
Nestin	AGGTGTCAAGGTCCAGGATG	AAGGAAGCAGACTCAGACCC
Gata4	AAACCAGAAAACGGAAGCCC	ATAGTGAGATGACAGCCCGG
Msx2	CCTATCAACTCACCCCTGCA	CATTCAGGAGCAGAGTTGGC
Hand1	CAGCTACGCACATCATCACC	GAAATCTGGGGCAGCATCAG
Gata2	GATGAATGGACAGAACCGGC	TTCTTCATGGTCAGTGGCCT
Ets2	GGCACCAAACTACCCCAAAG	GTCGTGGTCCTTGGGTTTTC
Cdx2	GAAACCTGTGCGAGTGGATG	CAGCCAGCTCACTTTTCCTC
Cyp11a1	CGAGTTCACAGGCTGCATAC	ACTCCGCTAACCACACAGAA
Gata3	CCCTTCTCCAAGACGTCCAT	CTTTCTCATCTTGCCTGGCC
Actin	AGCCATGTACGTAGCCATCC	CTCTCAGCTGTGGTGGTGAA
Hprt1	GAATCCTCTGGGAGACGACA	CGGAAAGCAGTGAGGTAAGC
Gadd45g	AAGCACTGCACGAACTTCTG	ACGTGAAATGGATCTGCAGC
Plk2	CTCCGGACAGACTCTCTTCC	CTAGGCTGCTGGGTTATCGA
Creb3	TGTCACCTTCCGAGAACTCC	GAACCCCTCCTTTTCGAAGC
Ccnb1	TTGTGTGCCCAAGAAGATGC	ACGTCAACCTCTCCGACTTT
Cdkn1a	GAGAAAACCCTGAAGTGCCC	GTTTGGAGACTGGGAGAGGG
Klf4	GACATCAATGACGTGAGCCC	TGGGCTTCCTTTGCTAACAC
Esx1	AAACTACCAGGAACCCGAGG	ATCAGAGGACGCATCAGGG
Zic1	TGAACATGGCTGCACATCAC	AGATGTGGTTGCTCTGCTCT
Cdkn2b	CTGCCACCCTTACCAGACC	GCAGATACCTCGCAATGTCA
Ccna1	ACAGACCCAAGGCTCACTAC	TCCAGGAAGTTGACAGCCAA
Hmga2	CAAGAGCCAACCTGTGAGC	ACGACTTGTTGTGGCCATTT

Ccnd1	ACTGACAACTCTATCCGGCC	CGGATGGTCTGCTTGTTCTC
Cdc6	TCCTCCTCCGCTCAAAGAAG	ATCCGGGACAGCTGTATTCA
Krt18	CTGGGGCCACTACTTCAAGA	ATCTACCACCTTGCGGAGTC
Tbx2	GCCTGGACAAGAAAGCCAAA	TGGTCAGCTTCAGTTTGTGG
Bmp2	CTGGGGCCACTACTTCAAGA	ATCTACCACCTTGCGGAGTC
Sox7	GAACACGCTGCCTGAGAAAA	AGGACGAGAAGAAGGTCTGC
Pax6	TCTGCAGGTATCCAACGGTT	GCAAAGATGGAAGGGCACTC
Ncam1	GAATCAGACGGCCATGGAAC	TGCTCTTCAGGGTCAAGGAG
Hesx1	TACATGCCCCAGATCTTCCC	TACTTCGACCTGGTTCTGGG
Neurod1	ATCAAAAGCCCAAGAGACGG	GGGTCTTGGAGTAGCAAGGT
Olig1	GCAGCCACCTATCTCCTCAT	CAAGTTCAGGTCCTGCATGC
Olig2	CTGCGCCTGAAGATCAACAG	CGTAGATCTCGCTCACCAGT
Esrrb	TCTCATCTTGGGCATCGTGT	AGTTTCTTGTACCTGCGCAC
Zfp296	ATTAGGGGCCATCATCGCTT	GCACAGCAACTTCCAAGGAC
Nr0b1	CTATGTGTGCGGTGAAGAGC	CCTTGAGTGTGATCAGACGC
Gbx2	TCCCGGCCATTTCGTCTAC	CTGGGGATCTGGTGGTGAG
Lefty2	CATCGACTCTAGGCTCGTGT	CGAAACGGACCAACTTGTGT
Primers_ChIP-qPCR (related to Figures. 3, 7 and S4)		
Gene Name	**5' Forward**	**5' Reverse**
Zic1	CCTTCAAGCTCAACCCCAGT	GGAACAGAAAGTCCCGGGTA
Esx1	CTAGAGTGAGGCCCTTACCC	AGAGAGTCTGGGAAAGGGGA
Klf4	GAAGGGAGAAGACACTGCGT	GCACTTAAGGCCGACTCAAG
Brachyury	GGGTCGCTATCTGTTCGTCT	TGACCTCTCCAAAGCCTCAG
Hand1	CAAGATCAAGACTCTGCGCC	TTCTTACTTACCCCAGCCCG
Sox17	ATACGCCAGTGACGACCAG	GTTCGTCTTTGGCCCACAC
Gata4	GGCCCGTGTAATCTCTCTGA	CGCAAGTTTCCGAGCCTATC
Cdx2	ACCATCACCCGCATCATCA	CATCCACTCGCACAGGTTTC
Tbx2	CCTTACGGCGGGTCAGATC	CAGGGAGAAGGTGTCGGAAG
Hprt1	GAATCCTCTGGGAGACGACA	CGGAAAGCAGTGAGGTAAGC
Pou5f1	CAGACCCTTGTAGTGCCTGA	AGGCCATCAGACACTAAGCA
Sox2	AGCTCGCAGACCTACATGAA	TGGAGTGGGAGGAAGAGGTA
Nanog	CGGCTCACTTCCTTCTGACT	CATGTCAGTGTGATGGCGAG

Table S3. Antibodies used in this study, related to Figures 1, 5, 7 and S1-S6.

Antibodies	**SOURCE**	**IDENTIFIER**
Rabbit anti-Rbbp4	Bethyl	A301-206A-A
Rabbit anti-Oct4	Cell Signaling Technology	83932S
Mouse anti-Sox2	Cell Signaling Technology	4900s
Mouse anti-Nanog	Abcam	ab214549
Rabbit anti-Rbbp7	Cell Signaling Technology	#4522
Mouse anti-Ezh1	Santa Cruz Biotechnology	sc-398767
Rabbit anti-Ezh2	Cell Signaling Technology	5246S
Goat anti-Suz12	Santa Cruz Biotechnology	sc-46264
Sheep anti-Eed	R&D systems	AF5827
Rabbit anti-Jarid2	Cell Signaling Technology	13594S
Rabbit anti-Aebp2	Cell Signaling Technology	14129S
Rabbit anti-Foxa2	Abcam	ab108422
Rabbit anti-Gata6	Cell Signaling Technology	5851S
Rabbit anti-Cdx2	Cell Signaling Technology	12306S
Rabbit anti-Flag	Sigma-Aldrich	F1804
Rabbit anti-HA	Santa Cruz Biotechnology	sc-805
Rabbit anti-Ring1b	Proteintech	16031-1-AP
Rabbit anti-H3K27me3	Cell Signaling Technology	9733S
Rabbit anti-H2AK119ub1	Cell Signaling Technology	8240S
Rabbit anti-H3	Cell Signaling Technology	14269S
Rabbit anti-phospho-RB(Ser780)	Cell Signaling Technology	8180t
Rabbit anti-phospho-RB(Ser807/811)	Cell Signaling Technology	8516T
Rabbit anti-RB	Abcam	ab181616
Rabbit anti-p21	Cell Signaling Technology	#64016
Mouse anti-ppRB	BD Pharmingen	G3-245
Mouse anti-Actin	Proteintech	60008-1-Ig
Alex594-conjugated donkey anti-mouse IgG	Cell Signaling Technology	8809s
Alex488-conjugated donkey anti-rabbit IgG	Cell Signaling Technology	4412s
Alex488-conjugated donkey anti-mouse IgG	Cell Signaling Technology	4408s
Alex594-conjugated donkey anti-rabbit IgG	Cell Signaling Technology	8889s

Table S4. Additional datasets used in this study, related to Figures 2 and 3.

RNA-Seq Datasets		
Gene Name	**SOURCE**	**IDENTIFIER**
Suz12	(Pasini et al., 2007)	GSE31354
Ezh2	(Das et al., 2015)	GSE58414
Eed	(Das et al., 2015)	GSE58414
Oct4	(Loh et al., 2006)	GSE4189
Sox2	(Ding et al., 2015)	GSE66736
Nanog	(Loh et al., 2006)	GSE4189
ChIP-Seq Datasets		

Gene Name	SOURCE
Suz12	(Ben-Porath et al., 2008)
Eed	(Ben-Porath et al., 2008)
H3K27me3	(Ben-Porath et al., 2008)

Supplemental Experimental Procedures

Cell Culture

Mouse Embryonic stem cells (mESCs) were grown on 0.1% gelatin-coated culture dishes in DMEM medium supplemented with 15% fetal calf serum (Gibco) (v/v), 1,000 U/ml leukaemia inhibitory factor (LIF), 100 U/ml penicillin, 100 U/ml streptomycin (Thermo), 2 mM L-glutamine (Invitrogen), 1:100 non-essential amino acids (Invitrogen) and 0.1 mM β-mercaptoethanol (Sigma-Aldrich). HEK293FT and mouse embryonic fibroblasts (MEFs) were cultured in DMEM media containing 10% fetal calf serum (Gibco) (v/v), 100 U/ml penicillin-streptomycin (Thermo). MEFs were derived from E13.5 embryos and cultured as previously described (Qin et al., 2010). All cell lines used in this study were maintained in a humidified incubator at 37 ℃ and 5% CO2.

Colony Formation, Alkaline Phosphatase Staining and Flowcytometry

For colony formation assay, trypsinized ESCs were seeded on mitomycin-treated feeder MEFs (about 1,000 cells per 10cm plate) and grown for 7 days before image acquisition by phase contrast microscope (Olympus TH4-200). ESC colonies were stained with Alkaline Phosphatase Detection Kit (Yeasen #40749ES60), according to the manufacturer's guidelines. After staining to reveal AP activity, the colonies were scored and the percentage of undifferentiated, mixed and differentiated colonies was calculated. (n=3; error bars indicate the mean ± s.d.). Cell cycle analysis was performed, as previously described (Zhao et al., 2018). The experiment was carried out in strict accordance with the manufacturer's instructions (Vazyme A411-01/02). In short, 2–5 ×10^6 ES cells were trypsinised, washed in PBS, and then fixed dropwise into ice-cold 75% ethanol overnight at 4 ℃. Whereafter, fixed cells were washed with PBS, incubated for 30 min at 37°C in precooling PBS containing 20μl RNase A Solution and stained with propidium iodide (PI) at 4 ℃ in dark for 30 min. For apoptosis analysis, Annexin V-FITC/PI apoptosis detection kit (Yeasen #40302ES60) was used. Briefly, 2–5 ×10^5 cells were harvested, washed and resuspended in 100μL binding buffer containing 5μl Annexin V-FITC and 10μl PI at room temperature in the dark for 10 min. Fluorescence intensities were acquired using a LSRFortessa flow cytometer (BD Biosciences). The data were analyzed by the ModFit LT software and FlowJo software, respectively.

Embryoid Body Formation Assay

For Embryoid body differentiation, the protocol, hanging drop assay in Qin et al. was used (Qin et al., 2012). In short, a proper number of ESCs were seeded to non-adherent Petri-dishes. Suspended drop ESCs were maintained in IMDM medium without LIF (15% fetal calf serum, 2 mM L-Glutamine, 100 U/ml Penicillin-Streptomycin, non-essential amino acids, 50 μg/mL Ascorbic acid, 200 μg/mL iron saturated holo-transferrin, sodium pyruvate, 450 μM monothioglycerol, and 0.1 mM β-mercaptoethanol) to generate embryoid bodies (EBs). Three days later, the EBs were maintained on a rotating shaker using suspension culture method. The medium was replaced every 2 days throughout the differentiation

procedure. Pictures of EB morphology at day 6 and 12 were taken by Olympus (TH4-200). Total RNA was extracted (Trizol, Invitrogen) at the indicated time points and analyzed by RT-qPCR. All RT-qPCR primer sequences are available in Table S2.

Teratoma Formation Assay

5 x 10^6 ES cells were trypsinized, washed with PBS and injected subcutaneously into the flank of 6-week-old nude mice (the Model Animal Research Center of Nanjing University [D000521] BALB/c-*Foxn1*^{nu}/Nju). Teratomas were surgically isolated from mice 4 weeks after injection for routine histological analysis. Firstly, for preparation of teratoma paraffin blocks, teratomas were transferred into 4% paraformaldehyde (PFA) overnight at 4℃. Then, tissue samples were dehydrated and embedded in paraffin. Finally, 5-μm-thick paraffin sections were deparaffinized and stained with hematoxylin and eosin (H&E) based on a standard protocol (Qin et al., 2012; Zhao et al., 2018). All paraffin-sections subjected to histological examination after H&E staining. Images were acquired with a microscope (Olympus DP73). All animal procedures were approved by the Institutional Animal Care and Use Committee (IACUC) of the Model Animal Research Center at Nanjing University.

Cloning and Plasmid Generation

For construction of expression vectors for *Rbbp4* with an N-terminal Flag tag, the full-length *Rbbp4* coding sequence was amplified by PCR using Phanta Max Super-Fidelity DNA Polymerase (Vazyme #P505-d1) with primers containing the Flag tag sequence (DYKDDDDK). Mutant *Rbbp4* constructs were generated by Quick-change II site-directed mutagenesis kit (Agilent). The PCR product was inserted into lentiviral vector as described previously (Qin et al., 2012). In the same way, Full-length ORFs of *Oct4*, *Sox2* and *Nanog* were amplified with primers containing C-terminal Flag-tag or HA-tag from cDNA generated from ESCs. All ORFs were subsequently inserted between the NotI and BamHI sites of lentiviral vectors by recombination using ClonExpress II One Step Cloning Kit (Vazyme #C112-01), in accordance with manufacturer's instructions. For generation of *Rbbp4* targeting vector, an ~4.3kb NotI-KpnI fragment containing ~1.3 kb upstream and ~1.6 kb downstream homology arms, FRT flanked Neo cassette, floxed exon 3 and the neomycin positive selection marker was inserted into pBS KS II vector. And all expression vectors and targeting vector were verified by sequencing to ensure no mutations were introduced in protein coding sequence.

Lentiviral Supernatant Production and Infection

Lentiviral production and delivery were performed as previously described (Qin et al., 2012). Lentiviral particles were generated by co-transfecting HEK293FT cells with the lentiviral expression vectors along with third-generation packaging plasmids using Lipofectamine 2000 (Life Technologies). Concentrated virus particles were used to infect target cells in the presence of polybrene (Sigma, final concentration of 8 μg/ml). 24 hours after infection, ES cells were selected with puromycin (4 μg/ml) for 3–5 days to generate stable cell lines.

Immunofluorescence

For immunofluorescence, ESCs were plated on glass slides pre-coated with poly-L-lysine solution (Sigma-Aldrich). Standard immunofluorescence staining protocols were followed. Briefly, ESCs were fixed in 4%(w/v) paraformaldehyde for 15 min at room temperature, washed with PBS and then permeabilised in 0.5% Triton X-100 in PBS for 20 min at room temperature. After three 3 min-washes

in PBS, cells were incubated for 30 min in blocking buffer (PBS, 10% (v/v) goat serum, 1% (w/v) BSA) to block nonspecific binding sites. Next, the primary antibodies were diluted to the appropriate concentration in blocking serum at 4℃ overnight. Primary antibodies used were the following: anti-SOX2 (1/200, #4900s, Cell Signaling Technology), anti-OCT4 (1/200, sc-5279, Santa Cruz Biotechnology), anti-FOXA2 (1/200, ab108422, abcam), anti-GATA6 (1/200, 5851S, Cell Signaling Technology), and anti-CDX2 (1/200, 12306S, Cell Signaling Technology). After three 3 min-washes with PBS, cells were incubated for 1h at room temperature in the dark with the secondary antibody conjugated to fluorophores (Alexa Fluor® 488 donkey Anti-Mouse IgG (H+L) Antibody, Alexa Fluor® 488 donkey Anti-Rabbit IgG (H+L) Antibody, Alexa Fluor® 594 donkey Anti-Mouse IgG (H+L) Antibody and Alexa Fluor® 594 donkey Anti-Rabbit IgG (H+L) Antibody, Cell Signaling Technology) diluted 1:1000 in PBS 1% (w/v) BSA. Subsequently, coverslips were counterstained with DAPI (4′,6-diamino-2-phenylindole) (1:2000) for 5 min for nuclear detection at room temperature in the dark. After several more washes, cells were imaged with Zeiss LSM 880 laser scanning confocal microscope at 63X magnification.

Quantitative Real-time PCR

Total RNA was extracted (Trizol, Invitrogen) from cells or EBs and cDNA was generated by reverse transcription PCR using HiScriptTM 1st Strand cDNA Synthesis Kit (Vazyme #R111-01) according to the manufacturer's instructions. Relative mRNA expression levels were determined by PCR using PowerUp™ SYBR® Green Master Mix (Invitrogen) on the StepOnePlus™ Real–Time PCR System (Applied Biosystems). Data were analyzed with the ddCt method, using *β-actin* as a normalizer. Detailed primer sequences for RT-PCR are provided in the Table S1.

Histone Extraction

Histone extraction was performed as previously described (Qin et al., 2012; Zhao et al., 2017). In brief, the cells were harvested, washed and resuspended in Triton Extraction buffer (TEB) (PBS containing 0.5% Triton X 100 (v/v), 2mM phenylmethylsulfonyl fluoride, 0.02% (w/v) NaN3). Then the cells were shaken on ice for 10 min with gentle stirring and centrifuged at 6500 g for 10 min at 4℃ to spin down the nuclei. Supernatant was discarded and the nuclei pellet was washed in TEB and resuspended in 0.2 N HCL overnight at 4℃. Then the nucleic solution was centrifuged and supernatant was collected, and neutralized HCL with 5M NaOH at 1/25 of the volume of the supernatant. Protein content was determined using the Bradford assay.

Western Blotting and Immunoprecipitations

Total protein lysates were obtained by lysing cells in RIPA buffer (50 mM Tris pH 8.0, 150 mM NaCl, 5 mM EDTA, and protease inhibitors) as described (Huang et al., 2018). Cell lysates were separated by SDS-PAGE and transferred to PVDF membranes. For immunoprecipitation assay, immunoprecipitations were performed as follows. Cells were harvested and resuspended in 1ml of IP lysis buffer (50 mM Tris–HCl pH 8.0, 150 mM NaCl, 1% TtitonX-100, 2 mM EDTA, Complete protease inhibitors). After a 30 min incubation on ice, anti-RBBP4 (A301-206A-A, Bethyl), anti-SUZ12 (sc-46264, Santa Cruz Biotechnology) and ANTI-FLAG® M2 Affinity Gel beads (A2220, Sigma) were added to lysates for immunoprecipitation. The lysates were incubated with rotation at 20 rpm at 4℃ overnight and centrifuged at 2000g for 5 min at 4℃. Beads were then washed two times with IP lysis buffer and high-salt buffer (50 mM Tris–HCl pH 8.0, 450 mM NaCl, 1% TtitonX-100, 2 mM EDTA, protease inhibitors),

respectively, and resuspended in 50 μl of SDS sample buffer (125 mM Tris–HCl pH 6.8, 2% SDS, 10% glycerol, 1 mg/ml bromophenol blue, 100 mM DTT, 2% β-mercaptoethanol) and boiled at 95 ℃ for 5 min. Samples were loaded on SDS-PAGE for western blot analysis. Detailed antibodies used in this study are provided in the Table S3.

RNA Sample Preparation and RNA-Seq

Total RNA was extracted from ESCs using TRIzol® Reagent according the manufacturer's instructions (Invitrogen) and genomic DNA was removed using DNase I (TaKara). Then high-quality RNA sample was quantified using the ND-2000 (NanoDrop Technologies). RNA purification, reverse transcription, library construction and sequencing were performed at Shanghai Majorbio Bio-pharm Biotechnology Co., Ltd. (Shanghai, China), as per the manufacturer's instructions (Illumina, San Diego, CA). Shortly, 1μg of total RNA was prepared following TruSeq™ RNA sample preparation Kit from Illumina (San Diego, CA) for RNA-seq transcriptome librariy construction. Then the library was subsequently sequenced with the Illumina Novaseq 6000. The raw sequencing data were aligned to mouse genome (Ensemble GRCm38.p5) with orientation mode using TopHat (version2.1.1) (Langmead and Salzberg, 2012). To identify differentially expressed genes (DEGs), the expression level of each transcript was calculated according to the fragments per kilobase of exon per million mapped reads (FPKM) method. RSEM (http://deweylab.biostat.wisc.edu/rsem/) (Li and Dewey, 2011) was used to quantify gene abundances. R statistical package software EdgeR (Empirical analysis of Digital Gene Expression in R) (Robinson et al., 2010) was utilized for differential expression analysis. RNA-seq data in this study were deposited to the Gene Expression Omnibus (accession number. GSE144155).

Chromatin Immunoprecipitation (ChIP)

ChIP was performed as described previously (Qin et al., 2012; Zhao et al., 2017). In brief, 10^7 ES cells were collected and cross-linked for 10 min at room temperature with 1% formaldehyde (Sigma). The cross-linking reaction was terminated by the addition of glycine (0.125 M) for 5 min at room temperature followed by cell lysis (50 mM Tris pH 8.0, 1% SDS, 10 mM EDTA, protease inhibitors) at 4˚C for 20 min. Sonication was performed on a Bioruptor (Diagenode), resulting in an average DNA fragment size of 200-500 bp. Before immunoprecipitation, a 50 μl aliquot of solubilized chromatin was transferred to a new microtube and stored at −20˚C as 'input'. The fragmented chromatin fragments were incubated overnight in dilution buffer (16.7 mM Tris pH 8.0, 0.01% SDS, 1.2 mM EDTA, 1.1% Triton X-100, 165mM NaCl, protease inhibitors) at 4 ℃ under rotation with the indicated antibodies ((anti-EZH2, 5246S, Cell Signaling Technology)(anti-SUZ12, ab12073, Abcam)(anti-EED, AF5827, R&D systems)(anti-RBBP4, A301-206A-A, Bethyl)(anti-H3K27me3, 9733S, Cell Signaling Technology)). After incubation, the beads coupled with immunocomplexes were then washed twice in low-salt buffer (twice) (150 mM NaCl, 20 mM Tris pH 8.0, 0.1% SDS, 1 mM EDTA, protease inhibitors), high-salt buffer (twice) (500 mM NaCl, 20 mM Tris pH 8.0, 0.1% SDS, 1 mM EDTA, protease inhibitors) and TE buffer (twice) (10 mM Tris pH 8.0, 0.25 mM EDTA, protease inhibitors). The immunocomplexes were eluted for 1h at 65˚C with 150 μl of elution buffer (1% SDS and 100 mM NaHCO3). Chromatin was decross-linked overnight in 0.3 M Nacl at 65˚C. The enriched DNA was treated with RNase A (0.2mg/ml) for 2 hr at 37 ℃, then Proteinase K (0.2mg/ml) for 3 h at 55 ℃. DNAs were then purified using DNA gel extraction kit (Axygen) for subsequent quantitative PCR or deep sequencing analyses. ChIP enrichment was analyzed by qPCR using specific primers for target genes and the data were normalized to input.

ChIP-Seq and Data Analysis

For ChIP-seq samples, cross-linking, sonication and IP were performed in *Rbbp4*$^{\Delta/\Delta}$ ESCs expressing RBBP4-Flag (*Rbbp4*$^{\Delta/\Delta}$*/WT*) or *Rbbp4*$^{F/F}$ ESCs expressing empty Flag vector (*Rbbp4*$^{\Delta/\Delta}$ */EV*) (control). Flag M2 antibody (1:1,000, catalogue number F1804, Sigma) was used in the ChIP assays. 5ng of qualified ChIP DNA were used to generate the sequencing library using a NEB kit and sequenced on the Illumina platform (HiSeq PE150). Quality filtered ChIP-seq reads were aligned to the reference genome (GRCm38/mm10) using the bowtie2 software package (version 2.1.0). Only uniquely and non-duplicate mapped reads were kept, then the reads coverage and depth were calculated by samtools. MACS2 was used to generate signal tracks files in BigWig format and normalized it to 1 million reads. The significantly enriched ChIP-seq peaks were identified by using MACS package with a P-value cutoff of 5×10^{-4}. Visualization of the mapped reads and peak calling was performed by bigwig files using IGV tools. MACS2 (version 2.1.1) was used to call peaks, and followed by peak annotation using bedtools. Differential analysis between treat and control samples was conducted using bedtools. ChIP-seq data presented in this study are accessible through GEO series accession number GEO: GSE155029.

Supplementary References

Ben-Porath, I., Thomson, M.W., Carey, V.J., Ge, R., Bell, G.W., Regev, A., and Weinberg, R.A. (2008). An embryonic stem cell-like gene expression signature in poorly differentiated aggressive human tumors. Nature genetics *40*, 499-507.

Das, P.P., Hendrix, D.A., Apostolou, E., Buchner, A.H., Canver, M.C., Beyaz, S., Ljuboja, D., Kuintzle, R., Kim, W., Karnik, R., *et al.* (2015). PRC2 Is Required to Maintain Expression of the Maternal Gtl2-Rian-Mirg Locus by Preventing De Novo DNA Methylation in Mouse Embryonic Stem Cells. Cell reports *12*, 1456-1470.

Ding, J., Huang, X., Shao, N., Zhou, H., Lee, D.F., Faiola, F., Fidalgo, M., Guallar, D., Saunders, A., Shliaha, P.V., *et al.* (2015). Tex10 Coordinates Epigenetic Control of Super-Enhancer Activity in Pluripotency and Reprogramming. Cell stem cell *16*, 653-668.

Huang, Y., Zhao, W., Wang, C., Zhu, Y., Liu, M., Tong, H., Xia, Y., Jiang, Q., and Qin, J. (2018). Combinatorial Control of Recruitment of a Variant PRC1.6 Complex in Embryonic Stem Cells. Cell Rep *22*, 3032-3043.

Langmead, B., and Salzberg, S.L. (2012). Fast gapped-read alignment with Bowtie 2. Nat Methods *9*, 357-359.

Li, B., and Dewey, C.N. (2011). RSEM: accurate transcript quantification from RNA-Seq data with or without a reference genome. BMC bioinformatics *12*, 323.

Loh, Y.H., Wu, Q., Chew, J.L., Vega, V.B., Zhang, W., Chen, X., Bourque, G., George, J., Leong, B., Liu, J., *et al.* (2006). The Oct4 and Nanog transcription network regulates pluripotency in mouse embryonic stem cells. Nature genetics *38*, 431-440.

Pasini, D., Bracken, A.P., Hansen, J.B., Capillo, M., and Helin, K. (2007). The polycomb group protein Suz12 is required for embryonic stem cell differentiation. Molecular and cellular biology *27*, 3769-3779.

Qin, J., Van Buren, D., Huang, H.S., Zhong, L., Mostoslavsky, R., Akbarian, S., and Hock, H. (2010). Chromatin protein L3MBTL1 is dispensable for development and tumor suppression in mice. J Biol Chem *285*, 27767-27775.

Qin, J., Whyte, W.A., Anderssen, E., Apostolou, E., Chen, H.H., Akbarian, S., Bronson, R.T., Hochedlinger, K., Ramaswamy, S., Young, R.A., *et al.* (2012). The polycomb group protein L3mbtl2 assembles an atypical PRC1-family complex that is essential in pluripotent stem cells and early development. Cell Stem Cell *11*, 319-332.

Robinson, M.D., McCarthy, D.J., and Smyth, G.K. (2010). edgeR: a Bioconductor package for differential expression analysis of digital gene expression data. Bioinformatics (Oxford, England) *26*, 139-140.

Zhao, W., Liu, M., Ji, H., Zhu, Y., Wang, C., Huang, Y., Ma, X., Xing, G., Xia, Y., Jiang, Q., *et al.* (2018). The polycomb group protein Yaf2 regulates the pluripotency of embryonic stem cells in a phosphorylation-dependent manner. The Journal of biological chemistry *293*, 12793-12804.

Zhao, W., Tong, H., Huang, Y., Yan, Y., Teng, H., Xia, Y., Jiang, Q., and Qin, J. (2017). Essential Role for Polycomb Group Protein Pcgf6 in Embryonic Stem Cell Maintenance and a Noncanonical Polycomb Repressive Complex 1 (PRC1) Integrity. J Biol Chem *292*, 2773-2784.